

Supporting Information for

Influence of Metal Coordination and Light Irradiation on Hierarchical Self-Assembly Processes

Kalathil K. Kartha,^a Naveen Kumar Allampally,^b Antiope T. Politi,^c Deepak D. Prabhu,^d Hayato Ouchi,^d Rodrigo Q. Albuquerque,^{c*} Shiki Yagai^{d,e*} and Gustavo Fernández^{a*}

^a Organisch-Chemisches Institut, Universität Münster, Corrensstraße 40, 48151 Münster, Germany

^b Institut für Organische Chemie, Universität Würzburg am Hubland, 97074 Würzburg, Germany

^c School of Pharmacy and Biomolecular Sciences, Liverpool John Moores University, Liverpool L3 3AF, United Kingdom

^d Department of Applied Chemistry and Biotechnology, Graduate School of Engineering, Chiba University, 1-33- Yayoi-cho, Inage-Ku, Chiba 263-8522, Japan

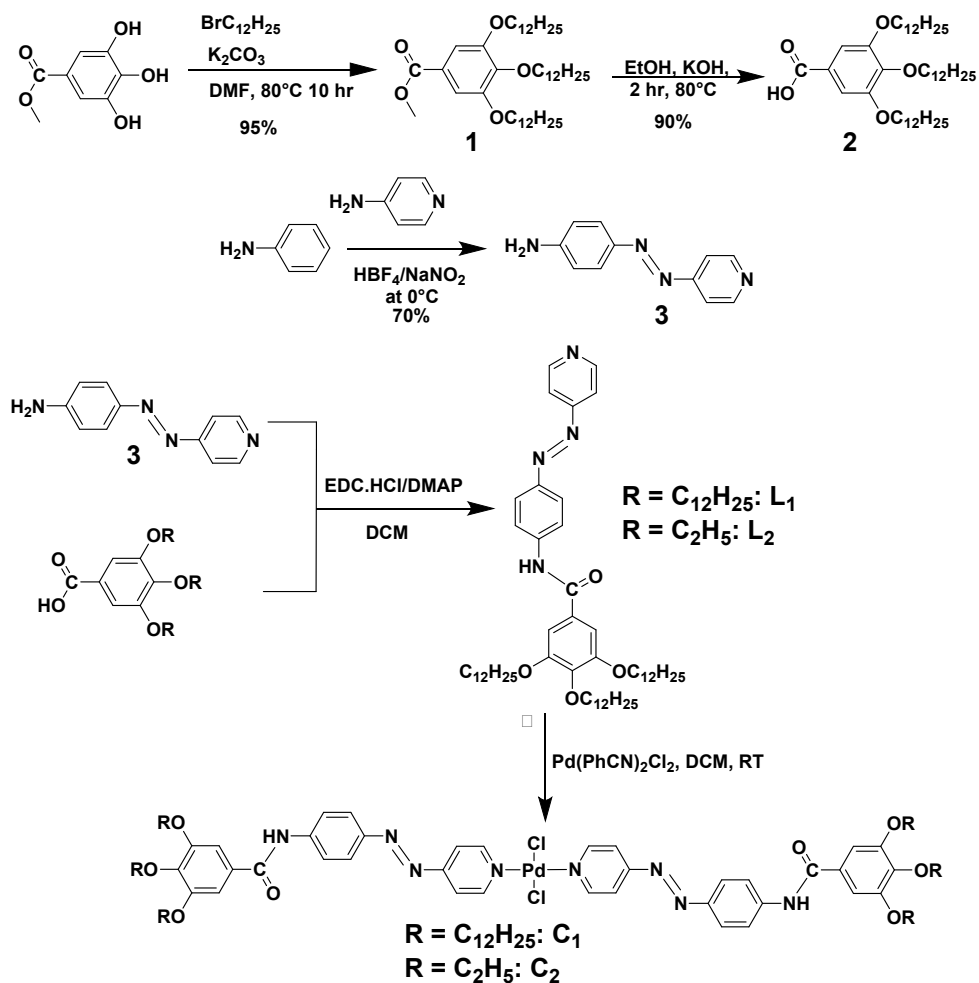
^e Institute for Global Prominent Research (IGPR), Chiba University, 1-33 Yayoi-cho, Inage-ku, Chiba 263-8522, Japan

CONTENTS

1. Experimental Section and Characterization Details.....	S3-S10
2. Description of Experimental Techniques	S10- S11
3. Supporting Figures, Tables and Schemes	S11-S32
4. References.....	S32

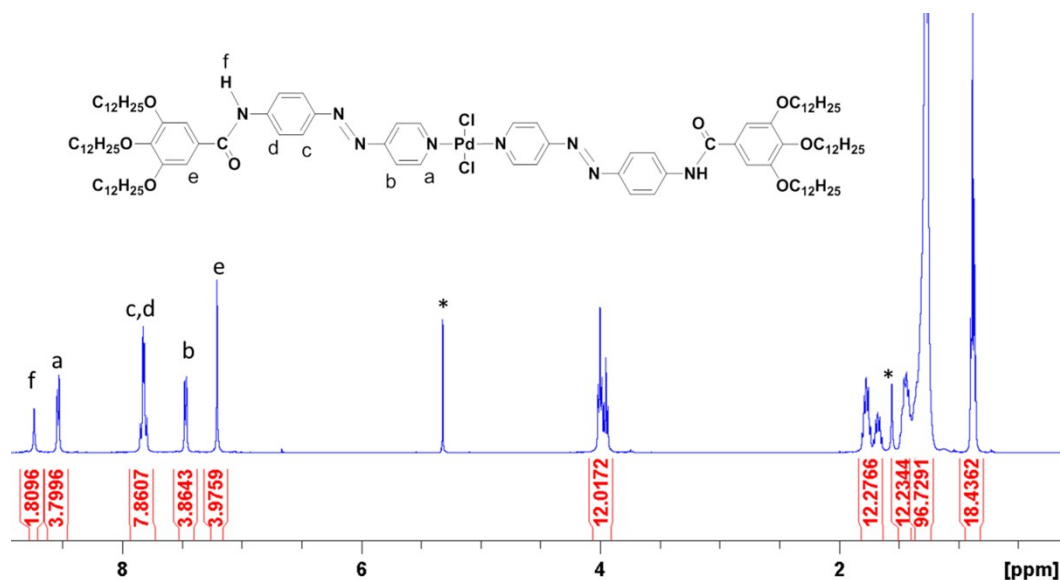
1. Experimental Section

The ligand **L**₁ and **L**₂ were synthesized by following a coupling reaction in the presence of EDC.HCl and DMAP in good yields. Metal complexes **C**₁ and **C**₂ were synthesized by reaction of ligands with Pd(PhCN)₂Cl₂ in dichloromethane (DCM) at room temperature.

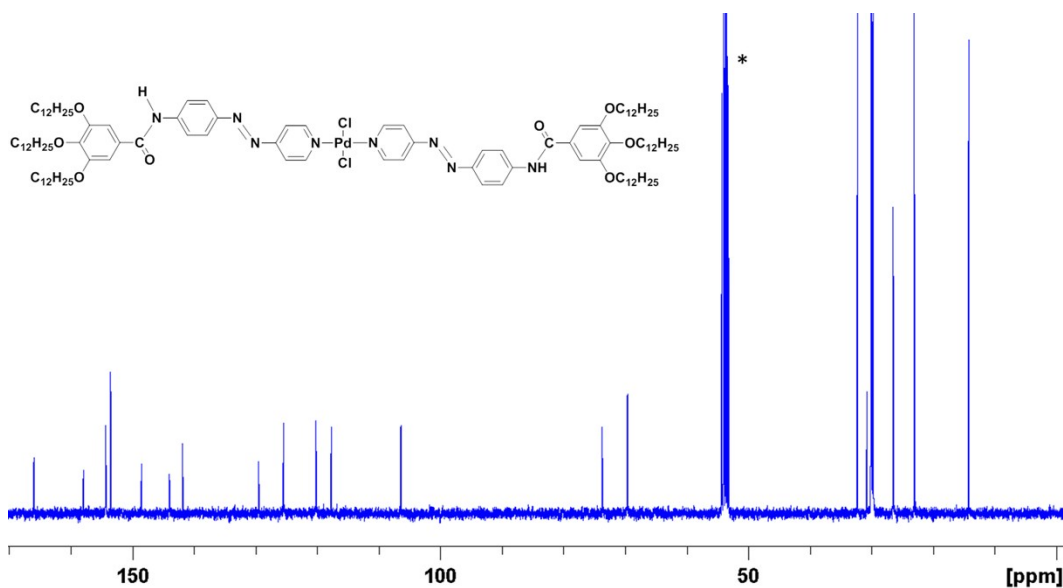


Scheme S1: Synthesis of ligands and corresponding Pd-complexes.

Synthesis of C₁: Compound L₁ (85 mg, 2 eq.) and Pd(PhCN)₂Cl₂ (19 mg, 1 eq.) were added to 30 mL of DCM. The reaction mixture was stirred at room temperature under N₂ overnight. The progress of the reaction was monitored by NMR. After 18 h, the ligand was completely consumed. The product was purified by 4 recrystallization cycles in EtOAc and MeOH. Yield: 80%. ¹H-NMR (400 MHz, CD₂Cl₂, 298 K): δ (in ppm) = 8.741 (s, 2H, H_f), 8.54 (d, J = 6.8 Hz, 4H, H_a), 7.937-7.727 (q, 8 H, H_{c,d}), 7.472 (d, J = 6.7 Hz, 4H, H_b), 7.21 (s, 4H, H_e), 4.063-3.912 (m, 12H, -O-CH₂-), 1.819-1.634 (m, 12H), 1.506-1.400 (m, 12H), 1.370-1.234 (m, 96H), 0.947-0.819 (m, 18H, -CH₃). ¹³C NMR (100.6 MHz, CD₂Cl₂, 298 K): δ (in ppm) = 166.2, 158.3, 154.6, 153.5, 148.8, 144.2, 141.9, 129.6, 125.9, 120.3, 117.8, 106.7, 73.9, 69.9, 32.4, 30.9, 29.9, 26.6, 23.2, 14.3. CHN Analysis: Calculated (C₁₀₈H₁₇₂Cl₂N₈O₈Pd), C, 68.71%; H, 9.18%; N, 5.94%; found C, 68.80%; H, 9.32%; N, 6.06%. FTIR (neat, cm⁻¹): 3277, 2918, 2850, 1661, 1583, 1519, 1500, 1468, 1444, 1425, 1403, 1385, 1336, 1303, 1239, 1209, 1143, 1118, 1055, 988, 850, 755, 718, 685, 654, 630, 564, 530.

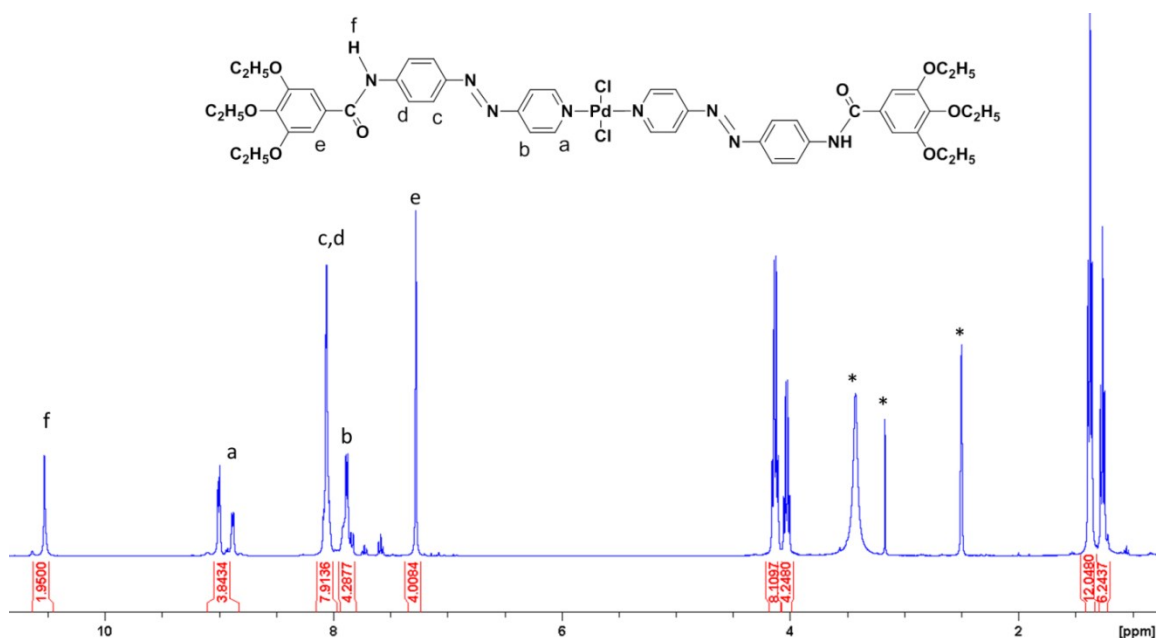


¹H-NMR spectrum of C₁ (400 MHz, CD₂Cl₂, 298 K).

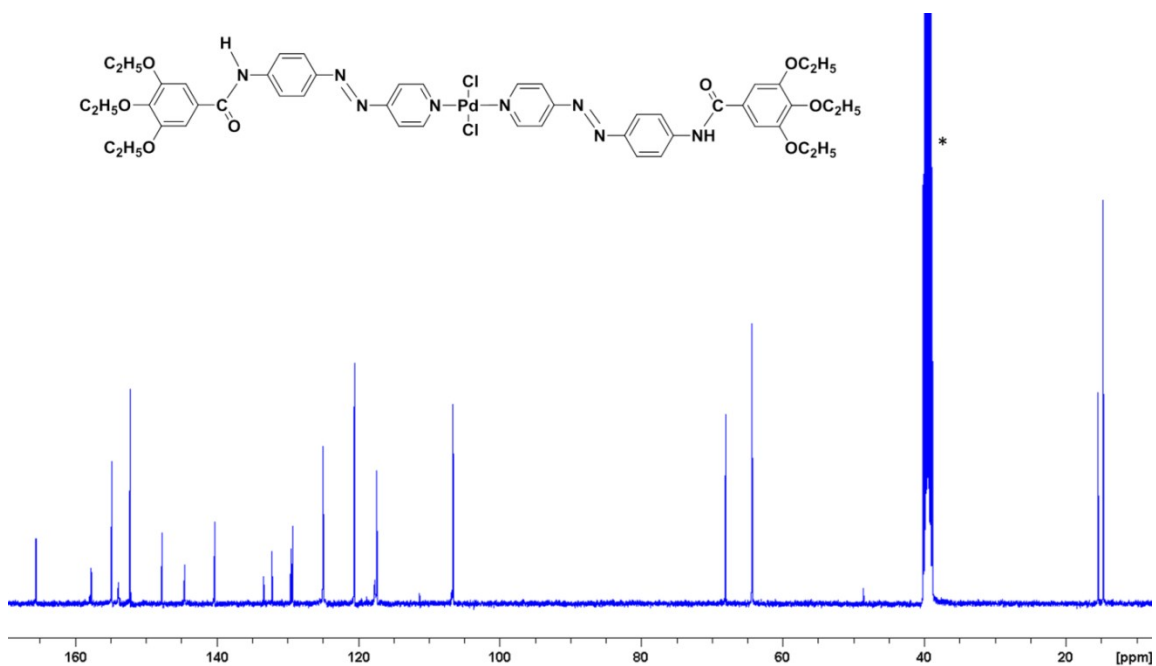


¹³C-NMR spectrum of C₁ (100.6 MHz, CD₂Cl₂, 298 K).

Synthesis of C₂: Compound L₂ (150 mg, 2 eq.) and Pd(PhCN)₂Cl₂ (65 mg, 1 eq.) were added to 50 mL of DCM. The reaction mixture was stirred at room temperature under N₂ overnight. The progress of the reaction was monitored by NMR. After 18 h, the ligand was completely consumed. The reaction mixture was concentrated in DCM and a huge excess of methanol was added. After keeping this mixture in fridge overnight, the precipitate that was obtained was filtered and dried. Yield: 92%. ¹H-NMR (400 MHz, DMSO-d₆, 298 K): δ (in ppm) = 10.547 (s, 2H, H_f), 9.107-8.828 (m, 4H, H_a), 8.153-7.970 (m, 8H, H_{c,d}), 7.873 (d, J = 6.8 Hz, 4H, H_b), 7.291 (s, 4H, H_e), 4.191-4.081 (m, 8H, -O-CH₂-), 4.075-3.988 (m, 4H, -O-CH₂-), 1.413-1.335 (m, 12H, -CH₃), 1.299-1.228 (m, 6H, -CH₃). ¹³C NMR (100.6 MHz, DMSO-d₆, 298 K): δ (in ppm) = 165.7, 157.8, 155.2, 153.9, 147.7, 144.5, 140.3, 133.5, 132.6, 129.5, 125.0, 117.5, 106.7, 68.2, 64.4, 15.5, 14.7. FTIR (neat, cm⁻¹): 3322, 3087, 2978, 2930, 2888, 1680, 1581, 1523, 1497, 1440, 1425, 1370, 1325, 1302, 1241, 1200, 1140, 1120, 1098, 1028, 980, 902, 848, 770, 750.

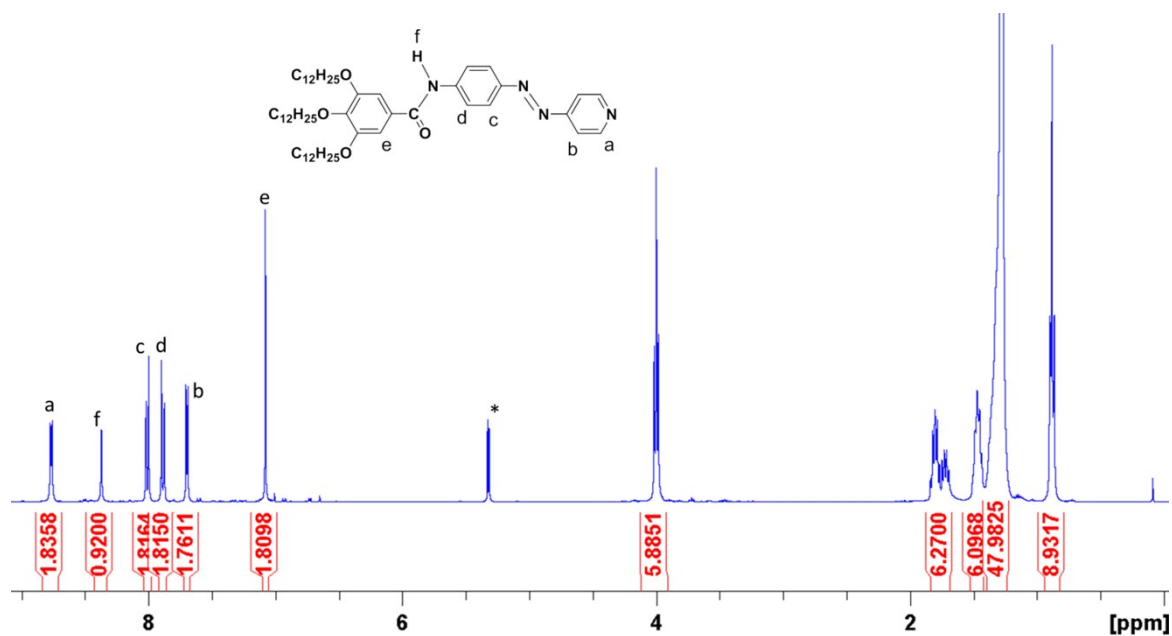


¹H-NMR spectrum of C₂ (400 MHz, DMSO-d₆, 298 K).

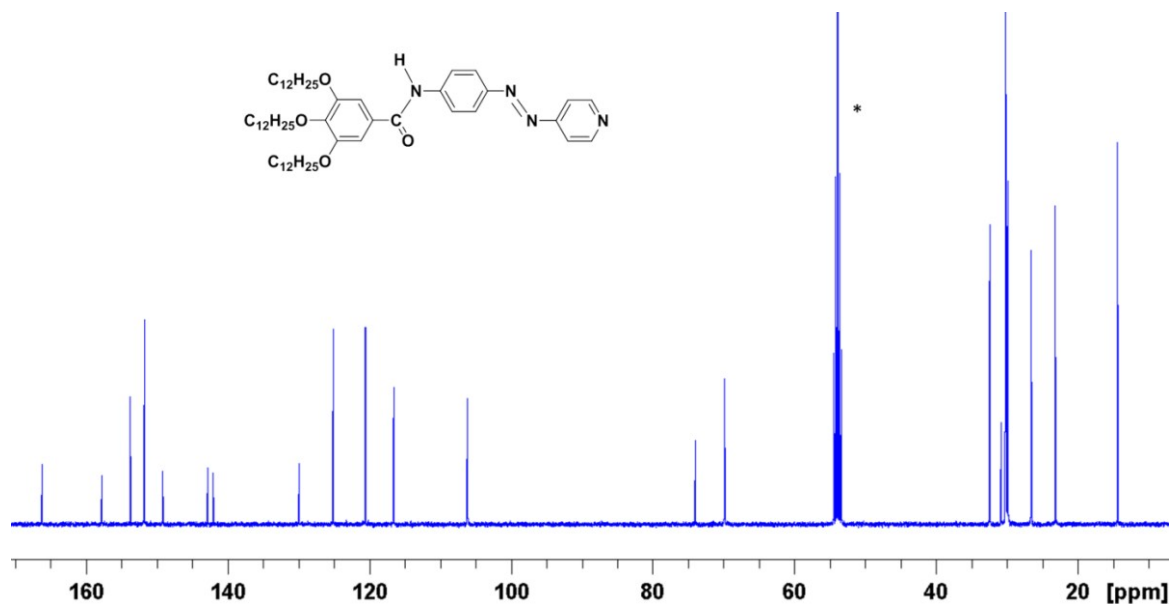


^{13}C -NMR spectrum of **C**₂ (100.6 MHz, DMSO-*d*₆, 298 K).

Synthesis of L₁: Compounds **2** (2.1 g, 1.5 eq.) and **3** (0.4 g, 1 eq.) were added into 20 mL of dry DCM under N₂ atmosphere. To this mixture, DMAP (0.172 g, 0.7 eq.) and excess of EDC (1.3 g, 3.36 eq.) were added and the reaction mixture was refluxed for 3 h. The progress of the reaction was followed by TLC. After cooling the reaction mixture, the crude product was extracted in DCM and washed with water (3 times). The organic phases were combined, washed with brine and dried over MgSO₄. Further, the pure product was obtained by column chromatography (Silica gel, 25% EtOAc in hexane). Yield: 65% (1.12 g). HRMS (ESI) *m/z*: Calculated, 855.67270 [M+H]⁺; found, 855.67207 [M+H]⁺. ¹H-NMR (400 MHz, CD₂Cl₂, 298 K): δ (in ppm) = 8.774 (d, *J* = 6.1 Hz, 2H, H_a), 8.374 (s, 1H, H_f), 8.012 (d, *J* = 8.5 Hz, 2H, H_c), 7.889 (d, *J* = 8.6 Hz, 2H, H_d), 7.700 (dd, *J* = 4.23, 1.65 Hz, 2H, H_b), 7.083 (s, 2H, H_e), 4.121-3.911 (m, 6H, -O-CH₂-), 1.843-1.690 (m, 6H), 1.531-1.425 (m, 6H), 1.401-1.238 (m, 48H), 0.944-0.822 (m, 9H, -CH₃). ¹³C NMR (100.6 MHz, CD₂Cl₂, 298 K): δ (in ppm) = 166.2, 157.7, 154.6, 153.8, 149.1, 142.8, 142.1, 129.6, 125.1, 120.5, 116.6, 106.1, 74.0, 70.1, 32.3, 30.8, 29.9, 26.5, 23.2, 14.3. FTIR (neat, cm⁻¹): 3302, 2919, 2849, 2356, 2334, 1651, 1584, 1520, 1500, 1470, 1448, 1425, 1406, 1384, 1338, 1301, 1239, 1212, 1118, 988, 878, 845, 832, 761, 719, 698, 674, 643, 560. Elemental analysis: Calculated (C₅₄H₈₆N₄O₄), C, 75.83%; H, 10.14%; N, 6.55%; found C, 75.55%; H, 10.13%; N, 6.35%.



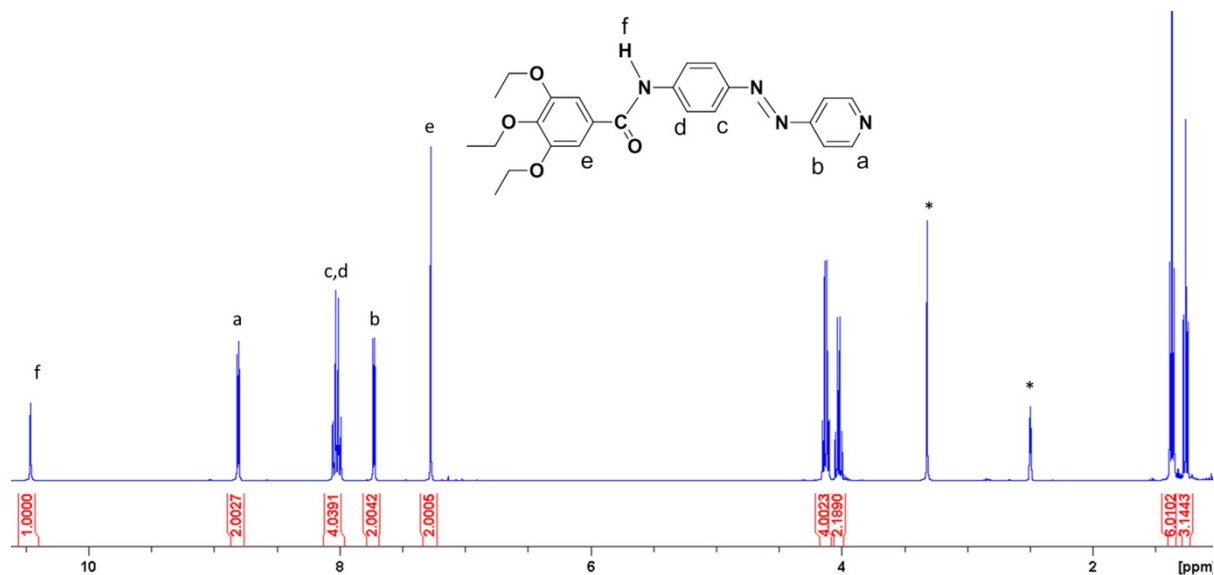
^1H -NMR spectrum of L_1 (400 MHz, CD_2Cl_2 , 298 K).



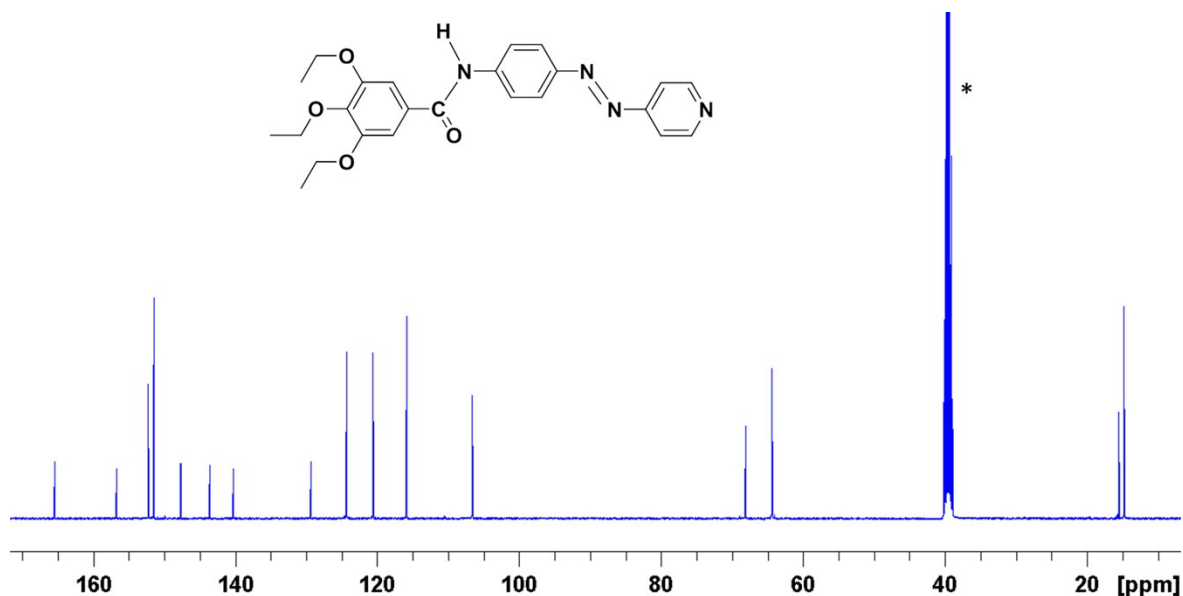
^{13}C -NMR spectrum of L_1 (100.6 MHz, CD_2Cl_2 , 298 K).

Synthesis of L_2 : The compound was synthesized by following the same procedure of L_1 using the corresponding acid with ethoxy instead of dodecyloxy chains. For the purification of the compound, column chromatography (Silica gel and 30% EtOAc in Hexane) was used. Yield: 81%. ^1H -NMR (400 MHz, DMSO-d_6 , 298 K): δ (in ppm) = 10.483 (s, 1H, H_f), 8.819 (d, $J = 6.1$ Hz, 2H, H_a), 8.134-7.961 (m, 4H, $\text{H}_{c,d}$), 7.741 (d, $J = 6.15$ Hz, 2H, H_b), 7.284 (s, 2H, H_e), 4.179-4.089 (m, 4H, $-\text{O}-\text{CH}_2-$), 4.067-3.990 (m, 2H, $-\text{O}-\text{CH}_2-$), 1.407-1.340 (m, 6H, $-\text{CH}_3$), 1.294-1.232 (m, 3H, $-\text{CH}_3$). ^{13}C NMR (100.6 MHz, DMSO-d_6 , 298 K): δ (in ppm) = 165.4, 156.9, 152.2, 151.4, 147.7, 143.7, 140.3, 129.4, 124.1, 120.5, 115.9, 106.6, 68.5, 64.4, 15.5, 14.7. FTIR (neat, cm^{-1}): 3284, 2972, 2926, 2875, 2354, 2330, 1644, 1580, 1514, 1444, 1431, 1389,

1371, 1336, 1305, 1244, 1216, 1153, 1120, 1029, 990, 900, 876, 844, 830, 763, 705, 672, 644, 671, 564. Elemental analysis: Calculated (C₂₄H₂₆N₄O₄), C, 66.34%; H, 6.03%; N, 12.89%; found C, 66.31%; H, 5.87%; N, 12.56%.



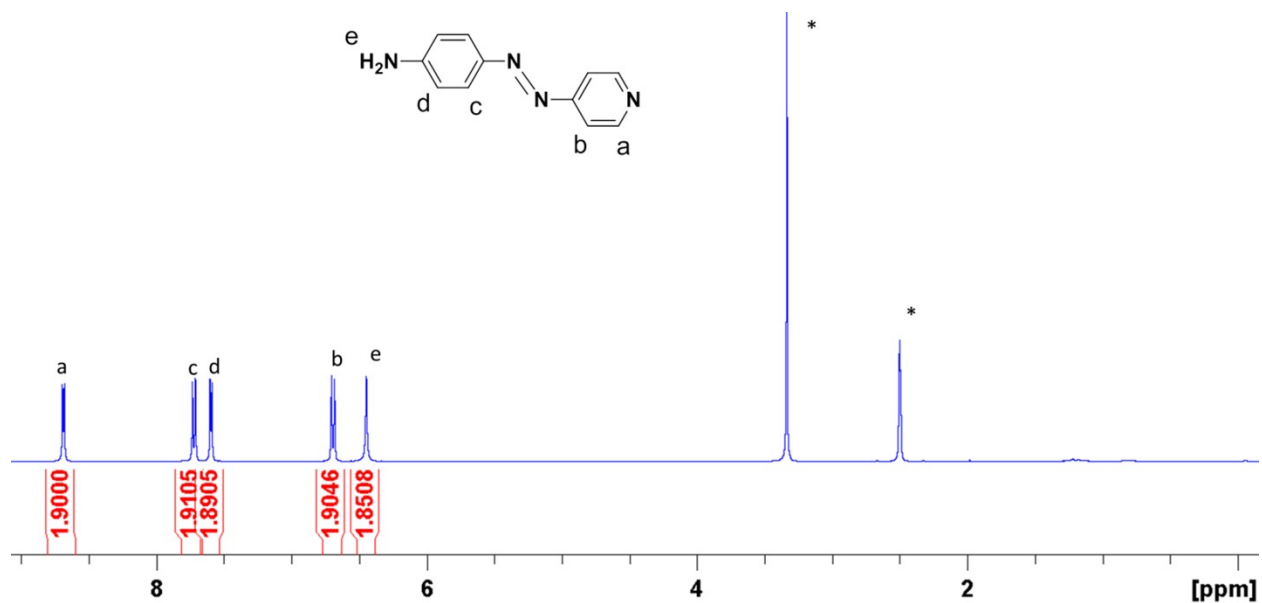
¹H-NMR spectrum of L₂ (400 MHz, DMSO-d₆, 298 K).



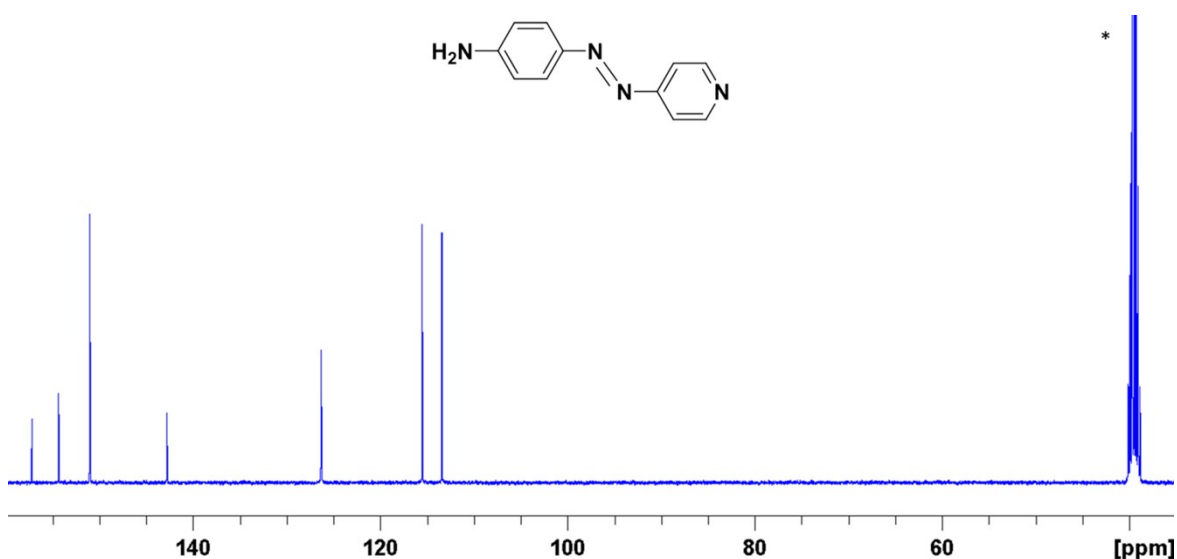
¹³C NMR spectrum of L₂ (100.6 MHz, DMSO-d₆, 298 K).

Synthesis of 3: 25 mL of HBF₄ was cooled in an ice bath and 4-aminopyridine (1.976 g, 1 eq.) was added. This mixture was stirred until a milky solution was obtained, to which NaNO₂ (7.45 g, 1 eq.) was added in small portions at 0°C. To the reaction mixture, aniline (3.9 mL, 2 eq.) was added very slowly. After addition, the reaction mixture was left stirring at room temperature for 2 h. The reaction mixture was neutralized with aqueous KOH under cooling conditions. The crude product was extracted in EtOAc and washed with water 3 times. The organic phases were combined, washed with brine and dried over MgSO₄. The product was purified by column chromatography (Silica gel, 25% EtOAc in hexane to 100% EtOAc). Yield: 70% (1.51 g). ¹H-NMR (400 MHz, DMSO-d₆, 298 K): δ (in ppm) = 8.69

(dd, $J = 4.23, 1.5$ Hz, 2H, H_a), 7.724 (d, $J = 8.83$ Hz, 2H, H_c), 7.597 (dd, $J = 8.5$ Hz, 2H, H_c), 7.889 (d, $J = 4.21, 1.53$ Hz, 2H, H_d), 6.695 (d, $J = 8.83$ Hz, 2H, H_b), 6.448 (s, 2H, H_e). ^{13}C NMR (100.6 MHz, DMSO-d_6 , 298 K): δ (in ppm) = 157.1, 154.3, 151.0, 142.9, 126.5, 116.2, 113.3.



^{13}C -NMR spectrum of **3** (100.6 MHz, DMSO-d_6 , 298 K).



^{13}C -NMR spectrum of **3** (100.6 MHz, DMSO-d_6 , 298 K).

Synthesis of 2: Compound **2** was synthesized by following a reported literature method. Methyl 3,4,5-trihydroxybenzoate (5 g, 1 eq.) and K_2CO_3 (30.8 g, 8 eq.) were mixed in 150 mL of dry DMF in a 250 mL round-bottom flask under N_2 gas. The mixture was stirred at room temperature for 1 h. After that, 1-bromododecane (29 mL, 4.1 eq.) was added and heated to 353 K and left stirring for 24 h under N_2 gas. The reaction mixture was cooled to room temperature and ice cooled water is added to it in order to precipitate the product. The product was further extracted in DCM and washed with water. Organic phases were added together and washed with brine and dried

over MgSO₄. The crude product was directly subjected to hydrolysis by refluxing in ethanol in excess of KOH. The reaction mixture was cooled to room temperature and was acidified (pH = 3-4). The solvent was evaporated and the crude compound **2** was extracted in DCM, washed with brine followed by drying over MgSO₄. The pure compound was obtained by column chromatography (Silica gel, 25% EtOAc to 50% EtOAc in hexane). Yield: 90%.

2. Description of Experimental Techniques:

General Procedures: All solvents were dried according to standard procedures. Reagents were used as purchased. All air-sensitive reactions were carried out under argon or nitrogen atmosphere. Mass spectra were recorded using electrospray ionization, performed on a MicroTof instrument (Bruker Daltronik GmbH) and on an Orbitrap LTQ XL (Thermo Scientific GmbH) in positive mode. NMR measurements: ¹H, ¹³C and 2D NMR spectra were recorded on a Bruker Avance 400 (¹H: 400 MHz; ¹³C: 100.6 MHz) or Bruker DMX 600 MHz spectrometer using partially deuterated solvents as internal standards. Coupling constants (*J*) are denoted in Hz and chemical shifts (δ) in ppm. Multiplicities are denoted as follows: s = singlet, d = doublet, t = triplet, m = multiplet. Chemical shifts are given in ppm relative to TMS (¹H, 0.0 ppm). Solvent and temperature-dependent ¹H NMR studies were investigated on Bruker DMX 500/600 MHz spectrometer using deuterated solvents.

UV/Vis measurements: UV/Vis absorption spectra were registered using a JASCO-V770 or JASCO-V750 spectrophotometer with a spectral bandwidth of 1.0 nm and a scan rate of 400 nm min⁻¹. Variable temperature measurements were performed with a ramp rate of 1K min⁻¹ unless otherwise specified. For all measurements, spectroscopic grade solvents were used. All experiments were carried out using quartz cuvettes with optical paths of 1 cm or 1 mm.

Atomic Force Microscopy: AFM images were recorded on a Multimode® 8 SPM System (AXS Bruker). Silicon cantilevers with a nominal spring constant of 9 Nm⁻¹ and with resonant frequency of ~150 kHz and a typical tip radius of 7 nm (OMCL-AC200TS, Olympus) were employed. The samples were prepared by spin coating of the corresponding aggregate solution onto a HOPG surface.

Photoirradiation Experiments were performed with a LSC-G HighPower-LED source emitting at 370 nm.

Quantum chemical calculations were carried out at the dispersion-corrected PM6^[s1] and Density Functional Theory (DFT) levels, where the geometry of up to tetramers of the Pd(II)-based *trans* complex and ligand alone (PM6) or monomer of the Pd(II)-based *cis* and both *trans* isomers (DFT) was optimized without any geometrical constraints in vacuum. The reliability of the optimized structures was confirmed by checking the absence of negative (imaginary) frequencies in the calculated vibrational spectra of the optimized structures. The excited states of the Pd(II)-based *cis* and both *trans* isomers was carried out *via* Time-Dependent DFT using the respective optimized ground state structures. The DFT calculations were done with the Gaussian09 program^[s2] using the PBE0 functional^[s3] and 6-31G* basis set for the light atoms, together with the LANL2DZ pseudopotential^[s4] for Pd(II). The semiempirical calculations were done with the MOPAC2016 program.^[s5]

The Molecular Dynamics (MD) simulations were carried out using the Gromacs program,^[s6] with the GAFF model and partial charges obtained from the semiempirical calculations. A stack of 270 molecules (39960 atoms) arranged in the antiparallel conformation was built and simulated at 300K and 1 atm using Periodic Boundary Conditions (PBC) and the NPT ensemble. A time step of 1 fs was used, together with the leap-frog integrator. The energy of the system was first minimized with the steepest descent algorithm (threshold force = 100 kJ.mol⁻¹.nm⁻¹). The Berendsen algorithm was used for both the thermostat and Barostat couplings (coupling constant of 2 ps). A cut-off of 1 nm was

used for the non-bonded interactions. Particle Mesh Ewald (PME) was used for the electrostatic interactions with a Fourier spacing of 0.16 nm. The system was relaxed for 1 ns before the production phase of 1 ns. No geometrical restrictions were used for the *trans* isomer, while for the *cis* isomer the torsion angle involving the azo nitrogens of all monomers was restricted to 0° using the LINCS algorithm (this angle is ca 180° for the *trans* isomers). All visualizations were done with the VMD program.^[s7]

Powder X-ray Diffraction (PXRD) Analyses were carried out using a Rigaku Rint-2200 X-ray diffractometer with monochromated $\text{CuK}\alpha$ radiation. The lattice parameters were refined using CellCalc ver. 2.10 software.^[s8]

3. Supporting Figures, Table and Scheme

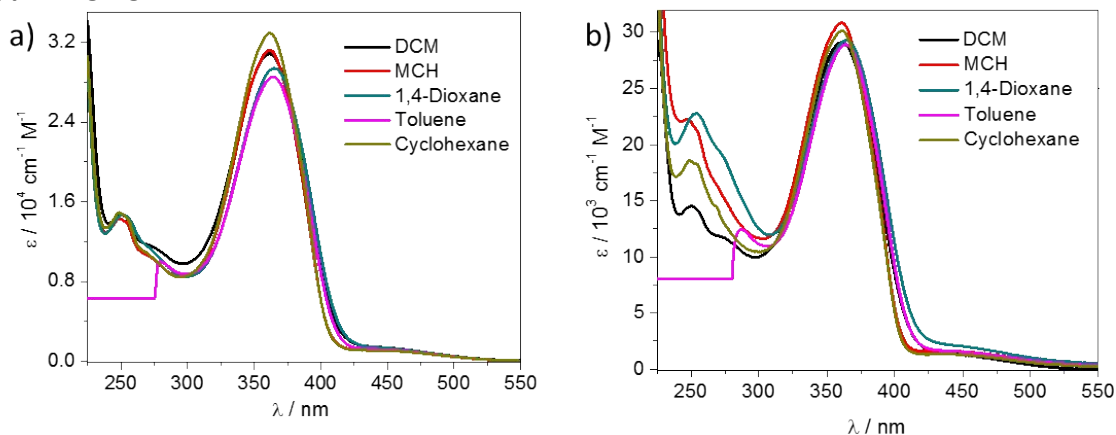


Fig. S1. Solvent-dependent UV-Vis spectroscopy of L_1 at a) $5 \times 10^{-4} M$ b) $1 \times 10^{-5} M$ at room temperature.

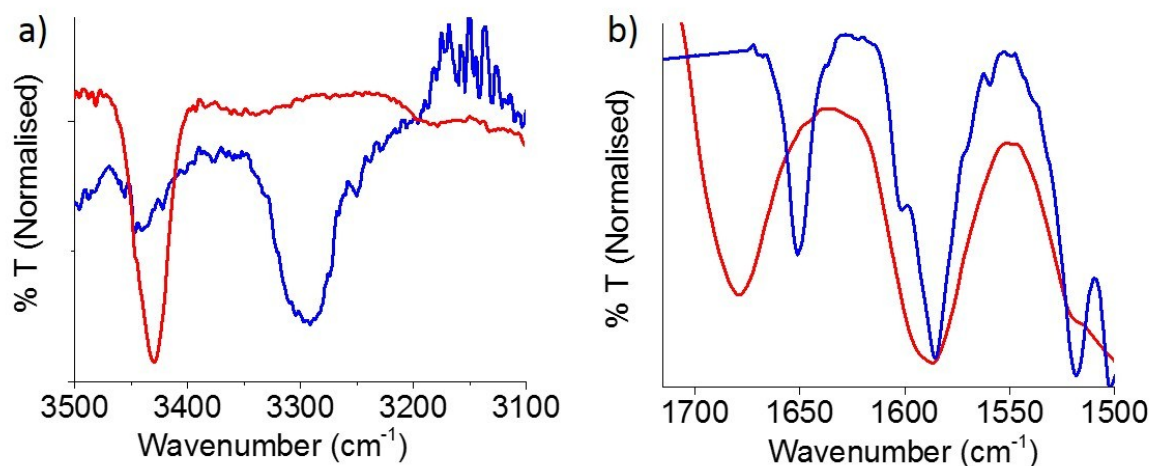


Fig. S2. FT-IR spectra of L_1 in a good solvent CHCl_3 (red) and bad solvent MCH (blue) with a conc. of $5 \times 10^{-4} M$ elucidating the intermolecular hydrogen bonding. Fingerprint corresponding to a) Amide I ($N-H$ stretching) in CHCl_3 (3430 cm^{-1}) and MCH (3285 cm^{-1}), and b) $C=O$ stretching in CHCl_3 (1680 cm^{-1}) and MCH (1650 cm^{-1}) showing monomeric L_1 in CHCl_3 and H-bonded L_1 assembly in MCH via $N-H \cdots O=C$ interaction.

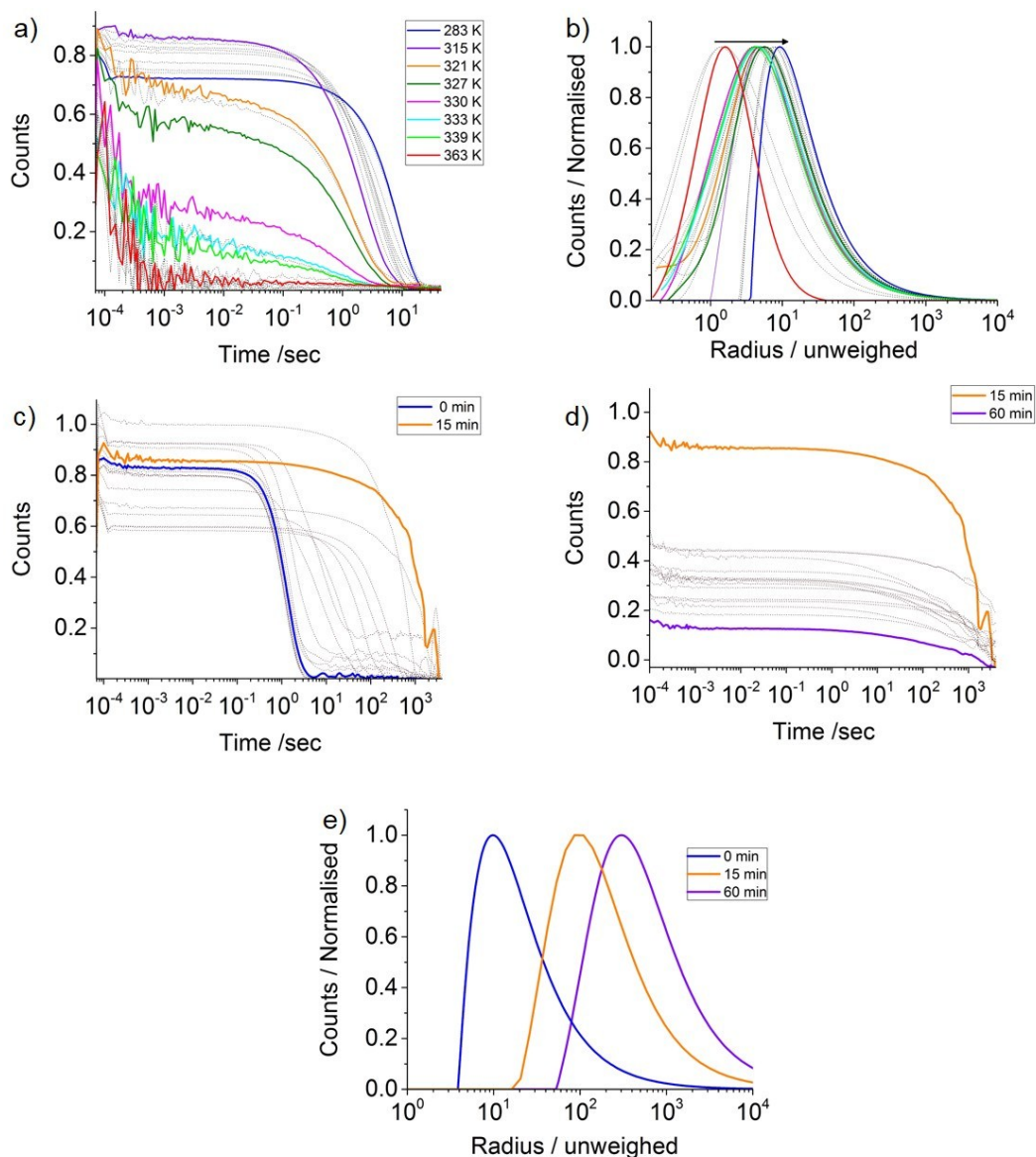


Fig. S3. a) Correlation function and b) corresponding size distribution (radius, unweighed) obtained from variable temperature DLS measurements from 363 K (red) to 283 K (blue) of L_1 with 5×10^{-4} M solution in MCH. The featureless correlation at 363 K in the plot a can be ascribed to the L_1 monomer with relatively high Brownian motion, while the observed decay from 5-10 sec at 283 K with good correlation function is in agreement with a L_1 dimer formation. The arrow in plot b indicates the size distribution from 1-10 nm (maximum) with long tail up to 100 nm during the cooling process indicating the formation of discrete species, possibly L_1 dimers. Negligible changes were observed for another 40-60 min at 283 K. This delay of 40-60 min was excluded from the time-dependent experiments by assuming it as the time for reaching the equilibrium before starting the elongation. A stable decay for 5 successive measurements were taken as the first measurement at 283 K, i.e. '0 min' in figure c and e. Such a time-dependent DLS measurement from 0-15 min (c) showed significant increase in the decay from 10 to 3000 sec due to the oligomerization of the discrete species into large objects and as expected subsequent supramolecular polymerization was observed from 15-60 min (d) with a decrease in relative counts indicating the sedimentation of polymers in solution phase. e) Size distribution (radius, unweighed) showing a gradual increase from 10 to 1000 nm regime, in accordance with the supramolecular polymerization.

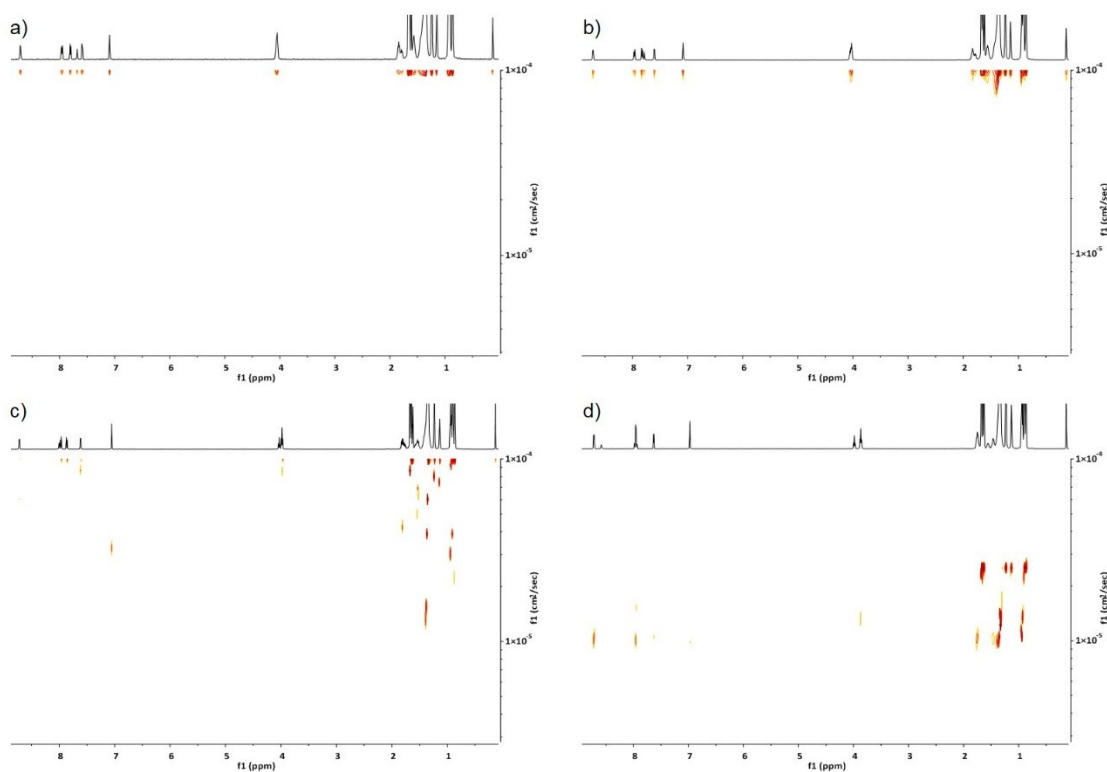


Fig. S4. Variable temperature DOSY-NMR measurement of L_1 with $5 \times 10^{-4} M$ solution in $MCH-d_{14}$ at a) 363 K, b) 343 K, c) 323 K and d) 298 K. The decrease in self-diffusion constant with cooling from 363 K to 298 K (from a-d) was in accordance with the possible discrete species formation such as dimers. But the calculated diffusion coefficient values (1×10^{-4} to $1 \times 10^{-5} cm^2 s^{-1}$) were not reliable and useful for further calculation of aggregates size.

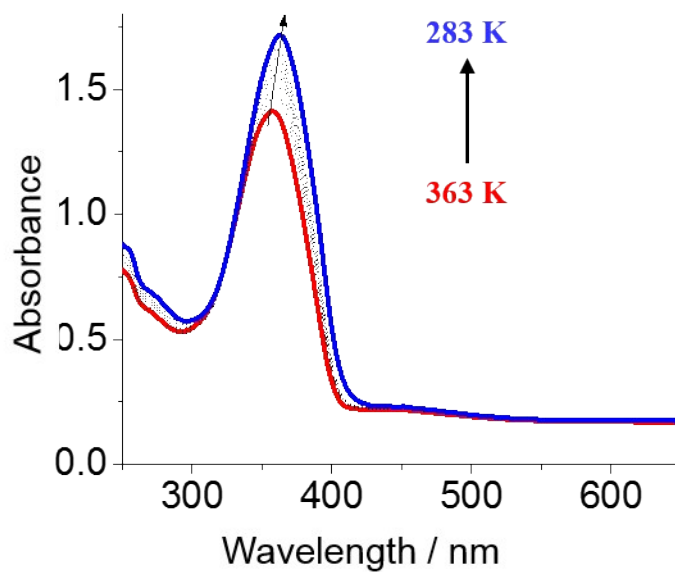


Fig. S5. VT-UV-Vis (from 363 K to 283 K) of L_1 at ($5 \times 10^{-4} M$) in MCH (l = 1 mm).

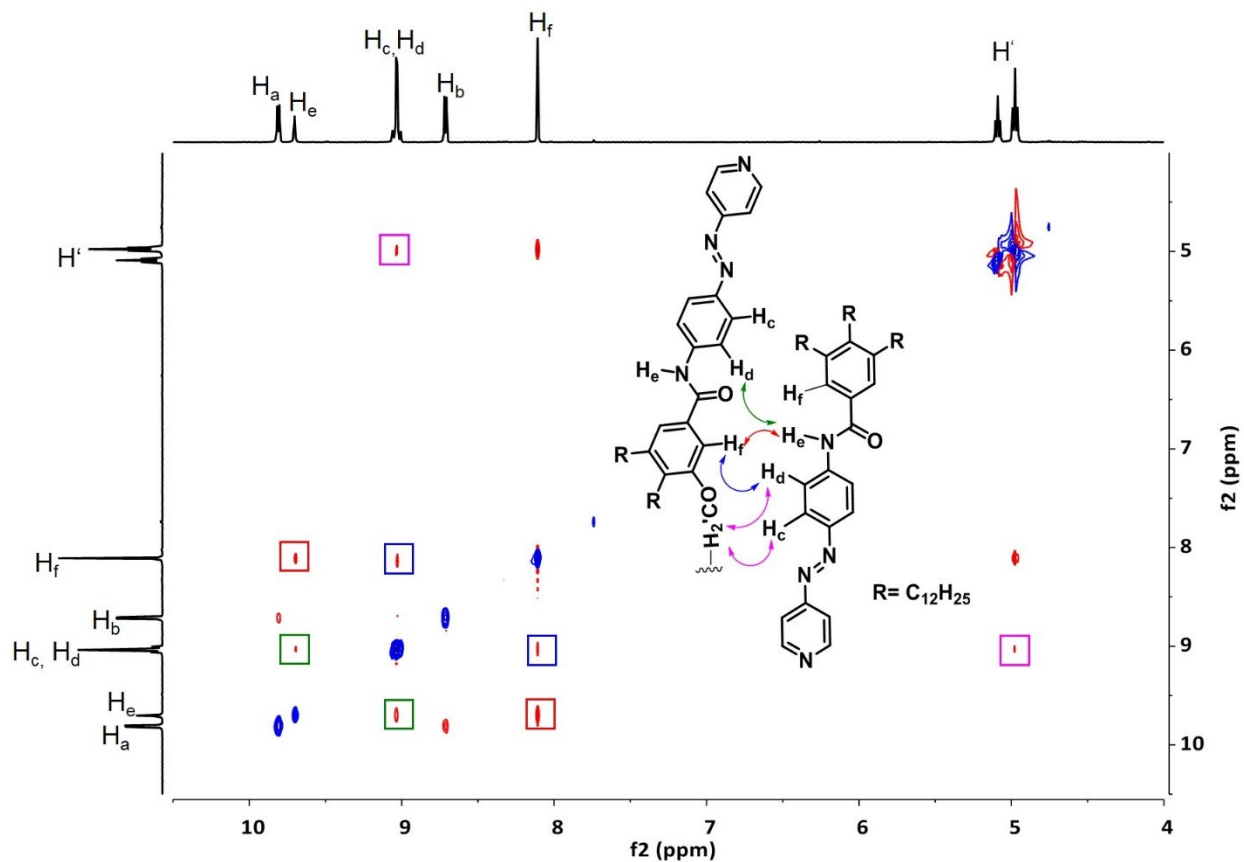


Fig. S6. Overlay of COSY (blue) and ROESY spectra (red) of L_1 (11.7 mM in $MCH-d_{14}$ at 315.32 K) showing the most relevant correlation signals. The observed coupling pattern (protons H_e and H_f (red box), $H_{c,d}$ and H_f (blue box), $H_{c,d}$ and H_e (green box) and H' ($-O-CH_2-$) and $H_{c,d}$ (pink box)) is in perfect agreement with VT-NMR and VT-UV-Vis (Figure 1 main text) results and support the stacking of the monomer units of L_1 in an antiparallel fashion in the aggregate structure (inset showing the possible spatial interactions).

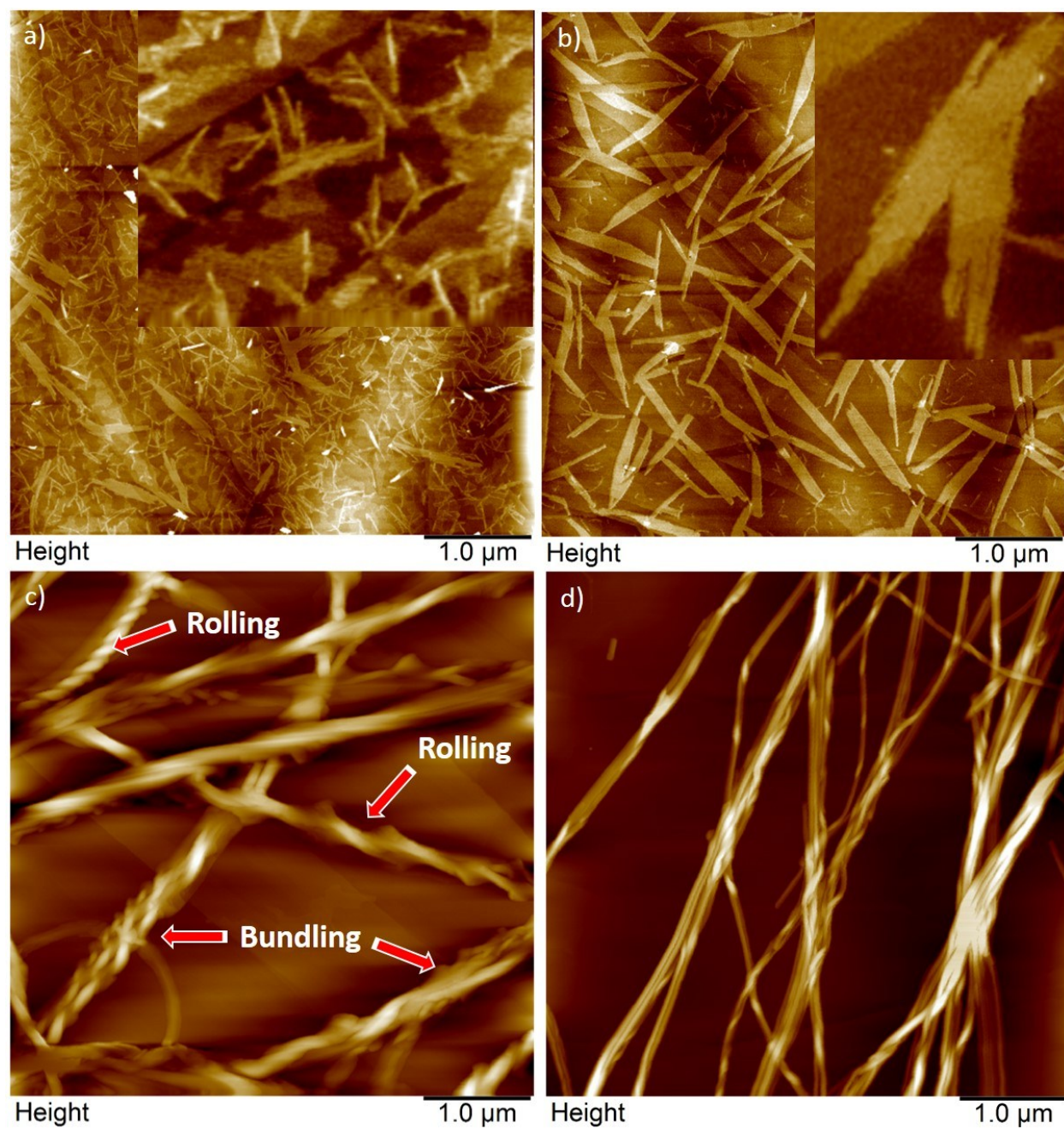


Fig. S7. Atomic force microscopy (AFM) images of self-assembled L_1 in MCH after keeping the solution at 283 K for: a) 15 min, b) 30 min, c) 45 min and d) 60 min (initial lag excluded) onto HOPG.

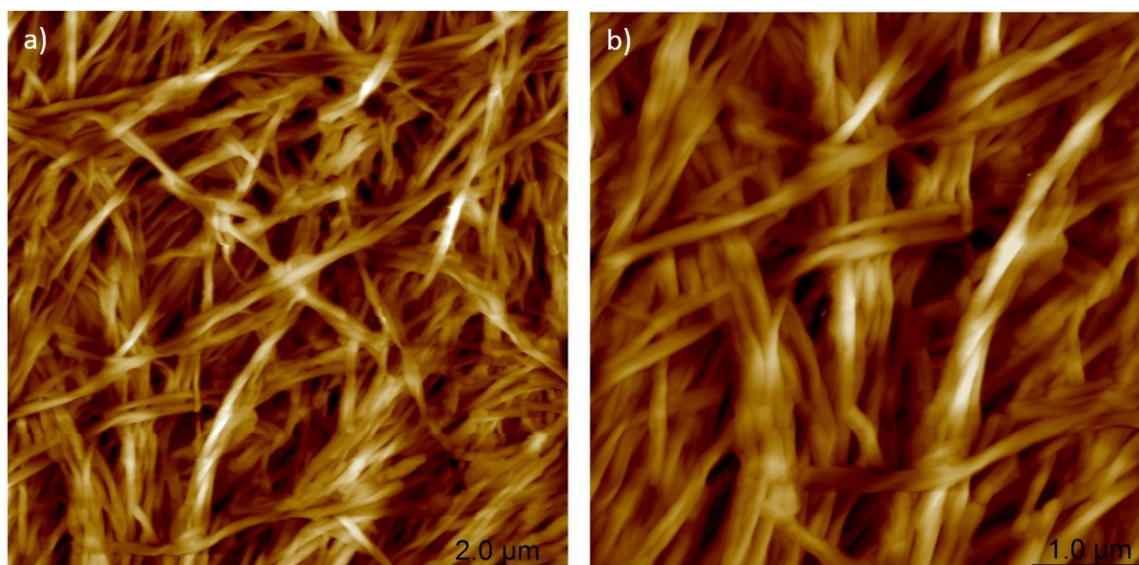


Fig. S8. AFM image of L_1 (5×10^{-2} M) aggregates in MCH at 298 K on HOPG.

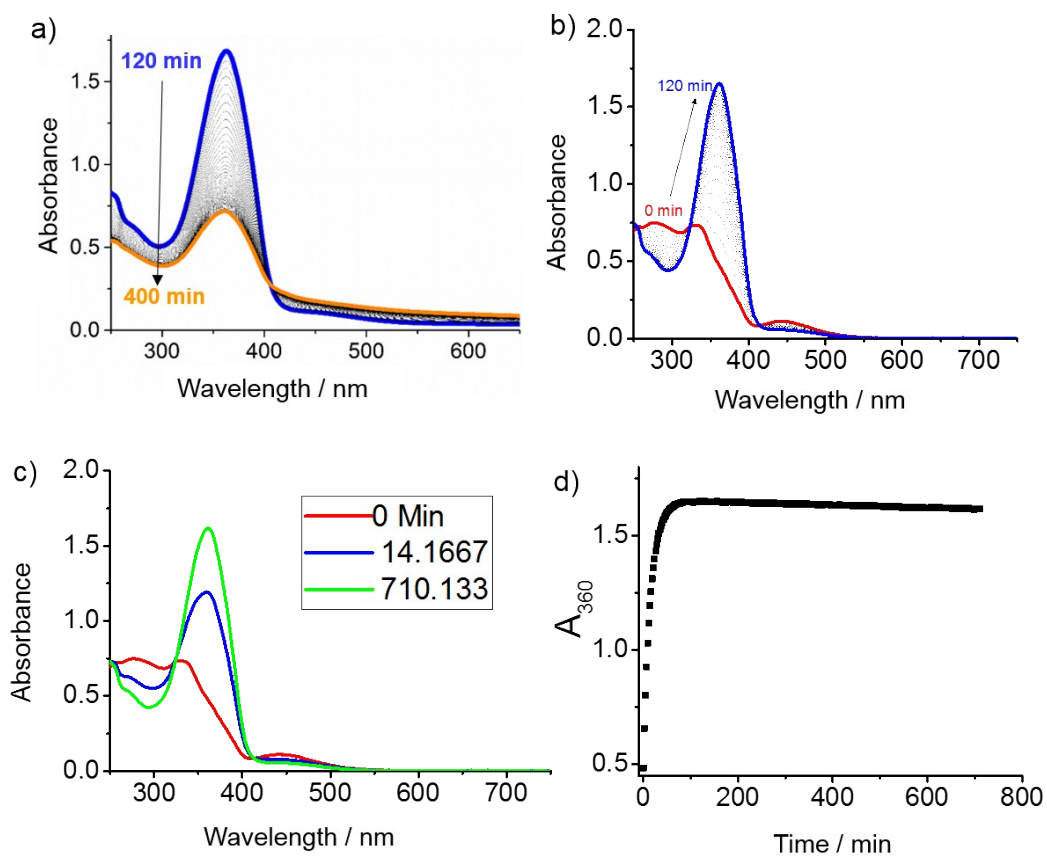


Fig. S9. Time-dependent absorption changes a) from 120 min to 400 min at 283 K, b) from 0 min to 120 min at 298 K, c) at different time intervals at 298 K, of L_1 (5×10^{-4} M) after irradiation for 30 min with a 365 nm LED lamp, d) A plot of A_{360} vs time (for 700 min) at 298 K. ($l = 1$ mm).

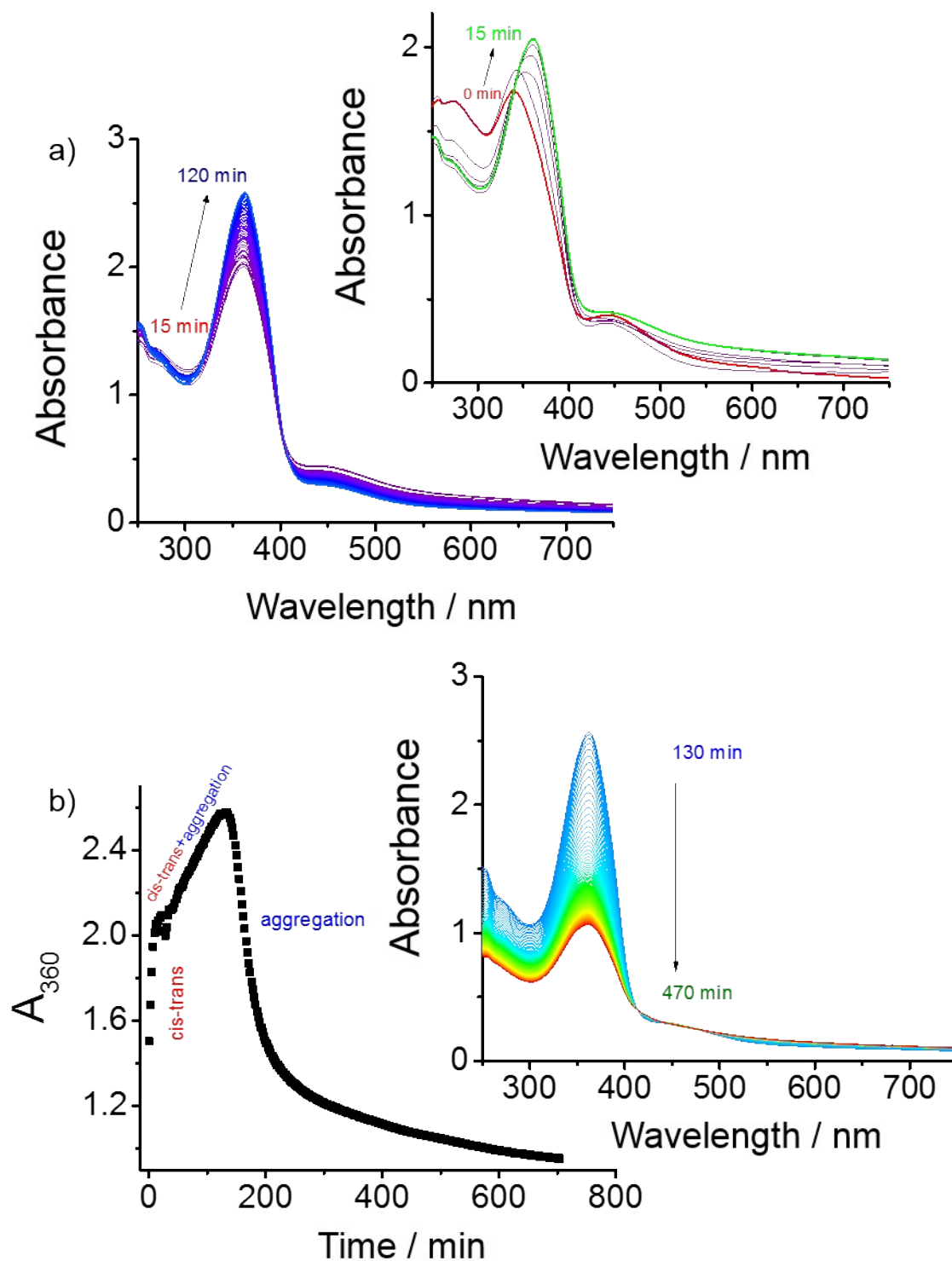


Fig. S10. a) Time-dependent absorption changes (from 15 min to 120 min) of L_1 (1×10^{-3} M) after irradiation for 30 min with a 365 nm LED lamp at 283 K (inset showing changes from 0 min to 15 min). b) A plot of A_{360} vs time (for 700 min) at 283 K (inset showing the absorption changes from 130 min to 470 min). ($l = 1$ mm).

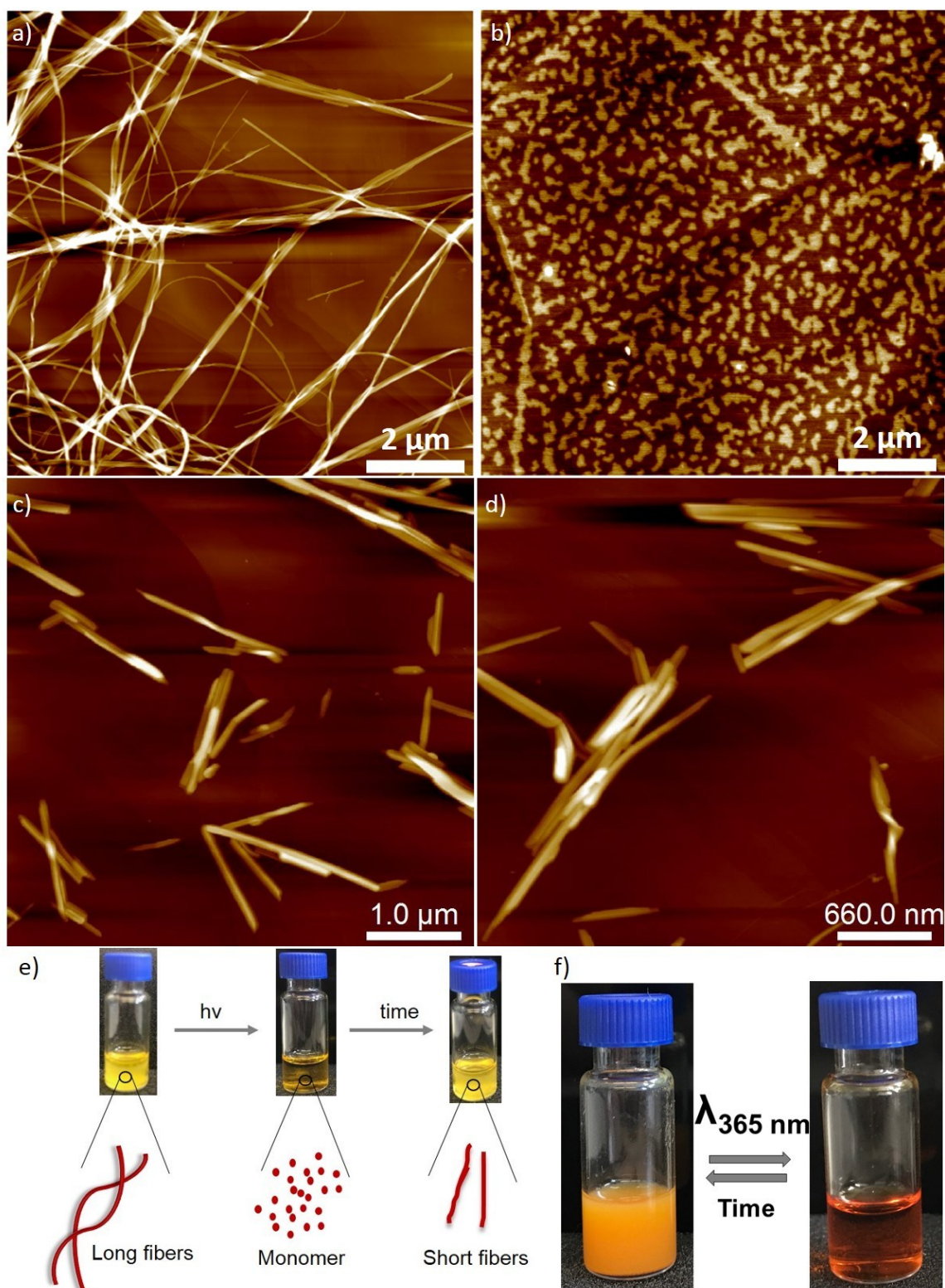


Fig. S11. AFM images of L_1 (5×10^{-4} M) aggregates formed in MCH at 283 K before (a), 140 min (b) and 800 min (c,d) after UV-irradiation for 30 min. e) Photographs and schemes showing the transition of L_1 (5×10^{-4} M) aggregates (long fibers) to monomer upon irradiation and subsequent photo reconstruction (to short fibers) over time (3-5 hrs at 283 K and 12-16 hrs at 298 K). f) Photographs showing the light-induced reversible gel-sol transition of L_1 .

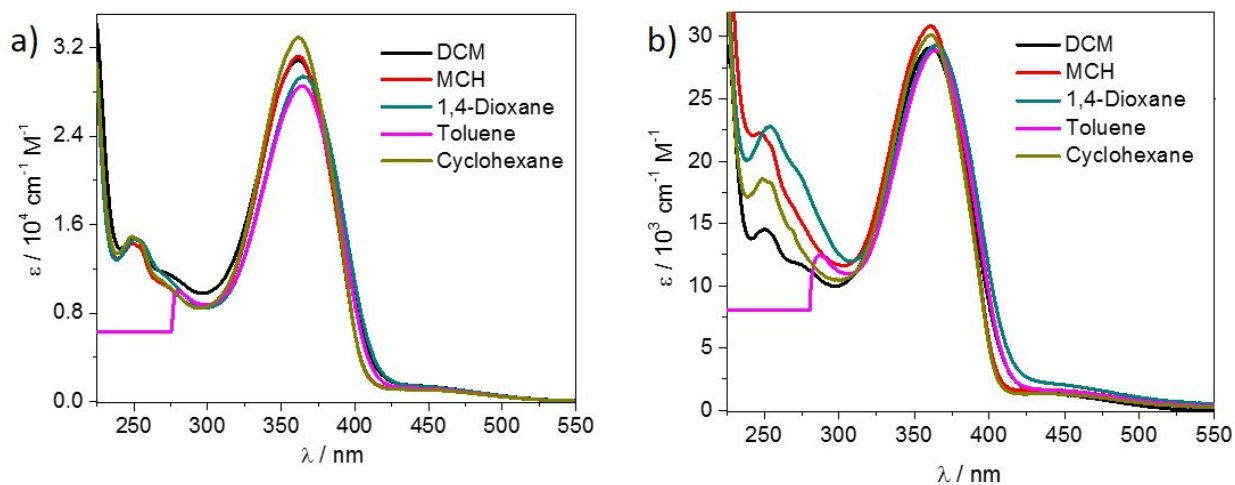


Fig. S12. Solvent-dependent UV-Vis studies of C_1 at a) 1×10^{-5} M and b) 4×10^{-4} M at room temperature ($l = 1$ cm).

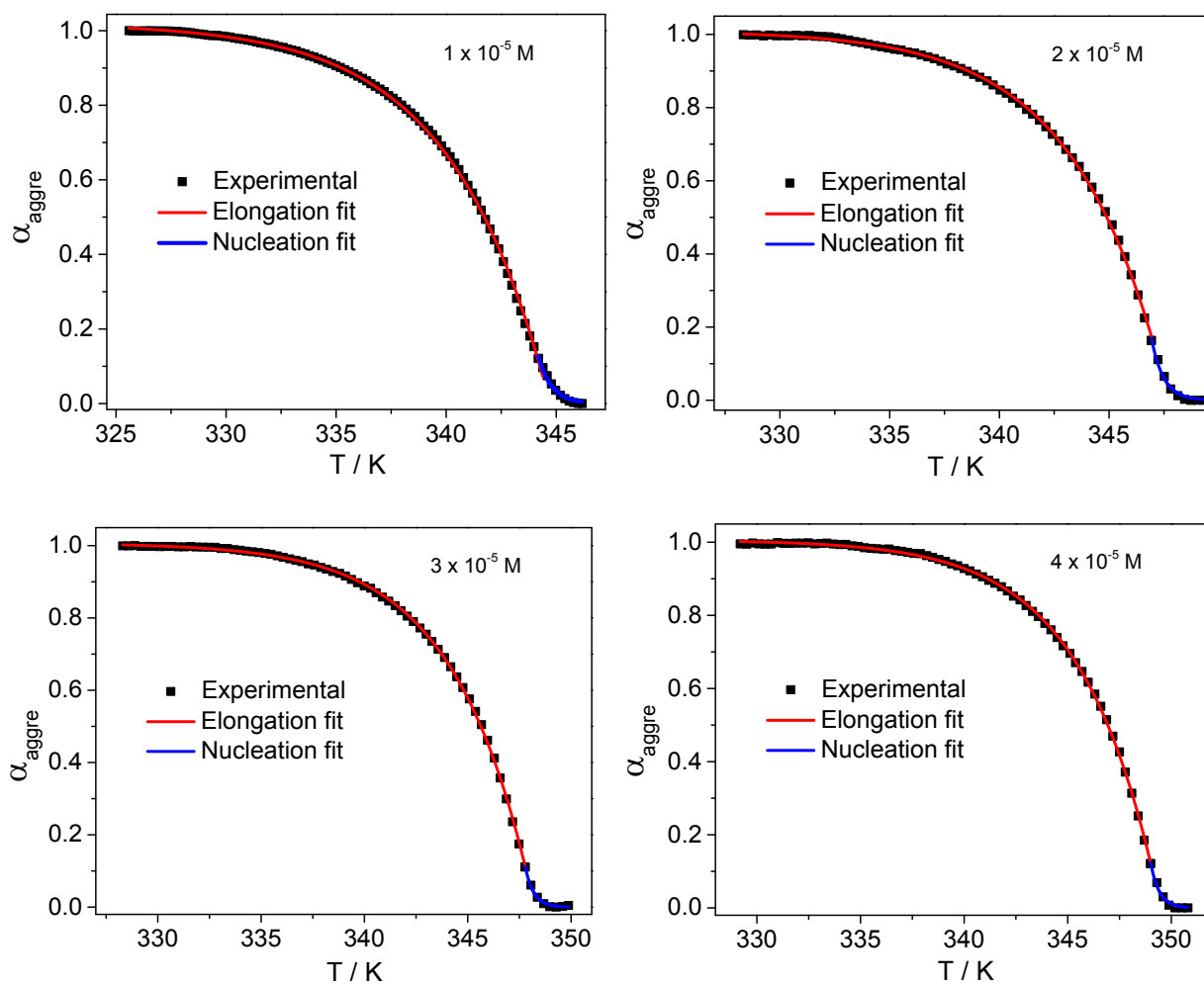


Fig. S13. Cooling curves of C_1 at different concentrations (1×10^{-5} , 2×10^{-5} , 3×10^{-5} and 4×10^{-5} M) obtained by monitoring the spectral changes at 395 nm.

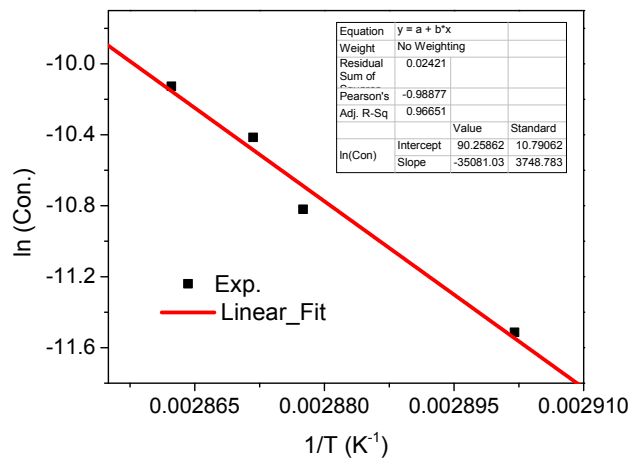


Fig. S14. Linear fit of logarithm of the concentration vs reciprocal elongation temperature for C_1 in MCH for 4 different concentrations between 1×10^{-5} M to 4×10^{-5} M.

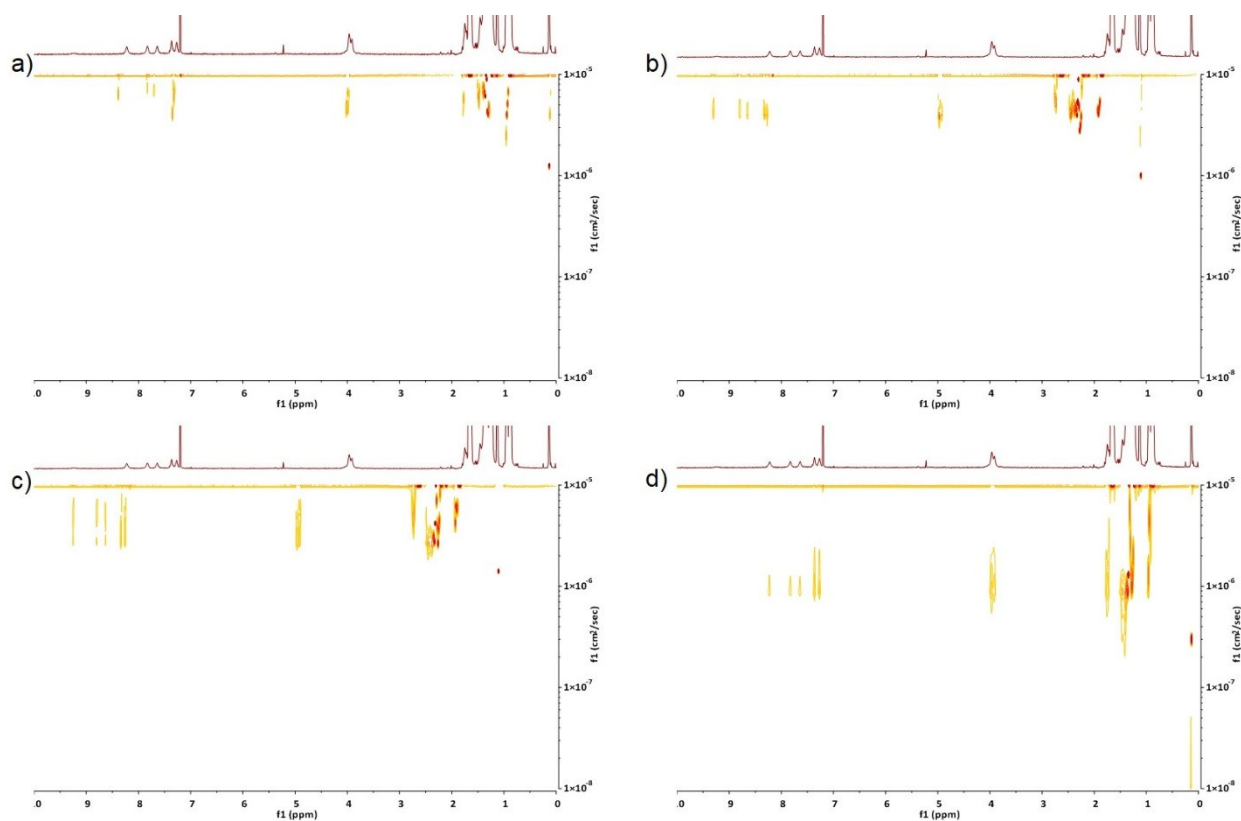


Fig. S15. Variable temperature DOSY-NMR measurement of C_1 with 5×10^{-4} M solution in MCH- d_{14} : $CDCl_3$ (9:1) at: a) 323 K, b) 313 K, c) 303 K and d) 298 K. The decrease in self-diffusion constant upon cooling from 323 K to 298 K (from a-d) is in accordance with an aggregation event.

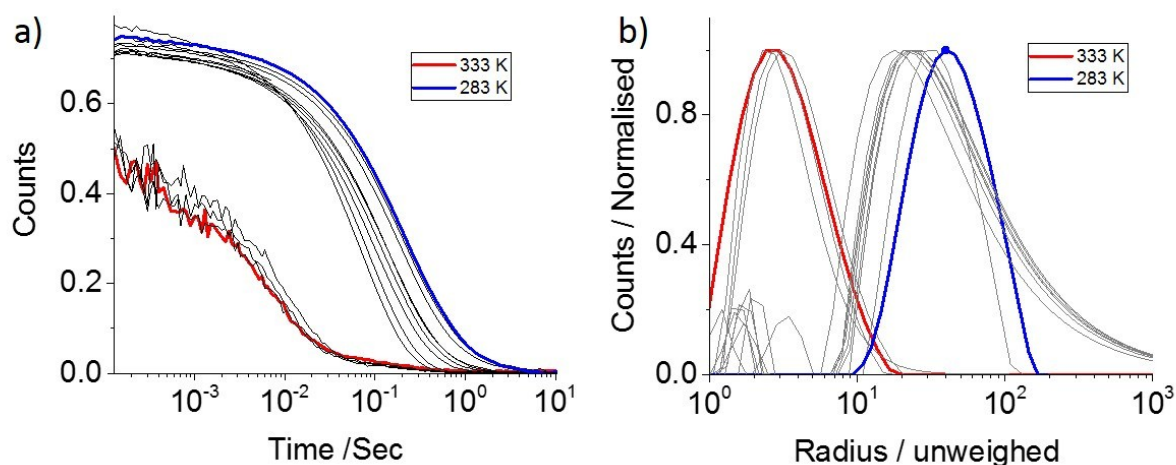


Fig. S16. a) Correlation function and b) corresponding size distribution (radius, unweighed) obtained from variable temperature DLS measurements from 333 K (red) to 283 K (blue) of C_1 with 5×10^{-4} M solution in MCH:CHCl₃ (9:1). The less defined correlation at 333 K (red) in plot a can be ascribed to the C_1 monomer with relatively high Brownian motion, while the observed decay at 283 K from 1-10 sec with good correlation function is in agreement with C_1 aggregate formation. The plot b showing the size distribution from 1-10 nm to 10-100 nm during the cooling process indicates the formation of supramolecular polymeric aggregates of C_1 .

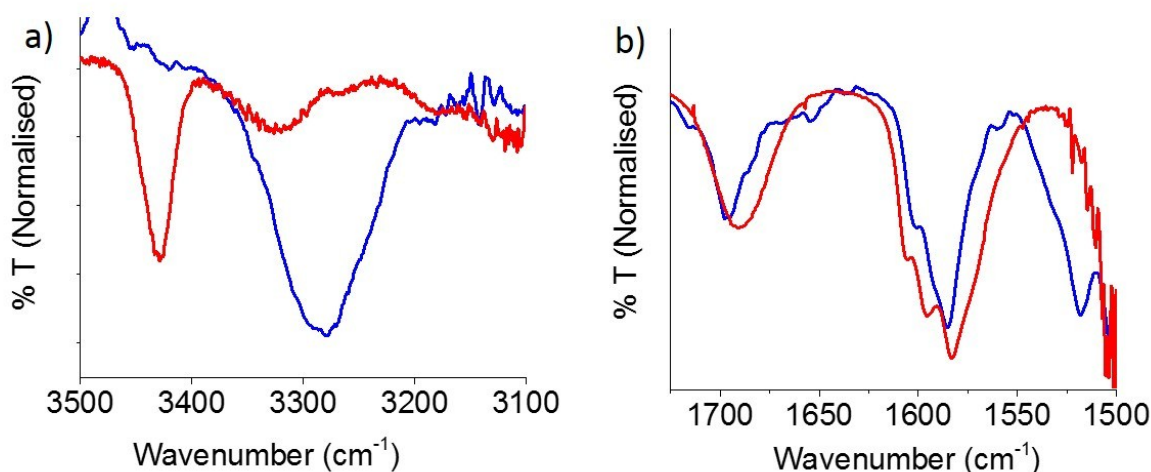


Fig. S17. FT-IR spectra of C_1 in a good solvent CHCl₃ (red) and bad solvent MCH (blue) with a conc. of 5×10^{-4} M elucidating the Pd-Cl...HN hydrogen bonding. Fingerprint corresponding to a) Amide I (N-H stretching) in CHCl₃ (~ 3430 cm⁻¹) and MCH (~ 3290 cm⁻¹) and b) C=O stretching in CHCl₃ (~ 1680 cm⁻¹) and MCH (~ 1685 cm⁻¹) showing a remarkable shift for N-H and negligible shift for C=O upon aggregation, which is in accordance with the Pd-Cl...HN driven assembly formation as reported previously by us (Macromol. Rapid Commun., 2018, 1800191).

Table S1. Thermodynamic parameters K_n , K_e , σ , T_e , ΔH° , N and α_{sat} obtained from the temperature-dependent UV-Vis experiments of C_1 (MCH, $\lambda = 395$ nm) on the basis of nucleation-elongation model.

Conc. (M)	N	ΔH° / kJ mol ⁻¹	α_{sat}	T_e / K	K_n	K_e	σ
1×10^{-5}	12	-223.00	1.0205	344.6	0.511	1×10^5	5.11×10^{-4}
2×10^{-5}	12	-243.64	1.0106	347.5	0.251	5×10^6	5.01×10^{-4}
3×10^{-5}	15	-266.83	1.0074	348.2	0.092	3.3×10^6	2.77×10^{-4}
4×10^{-5}	15	-273.74	1.0065	349.4	0.077	2.5×10^6	3.07×10^{-4}

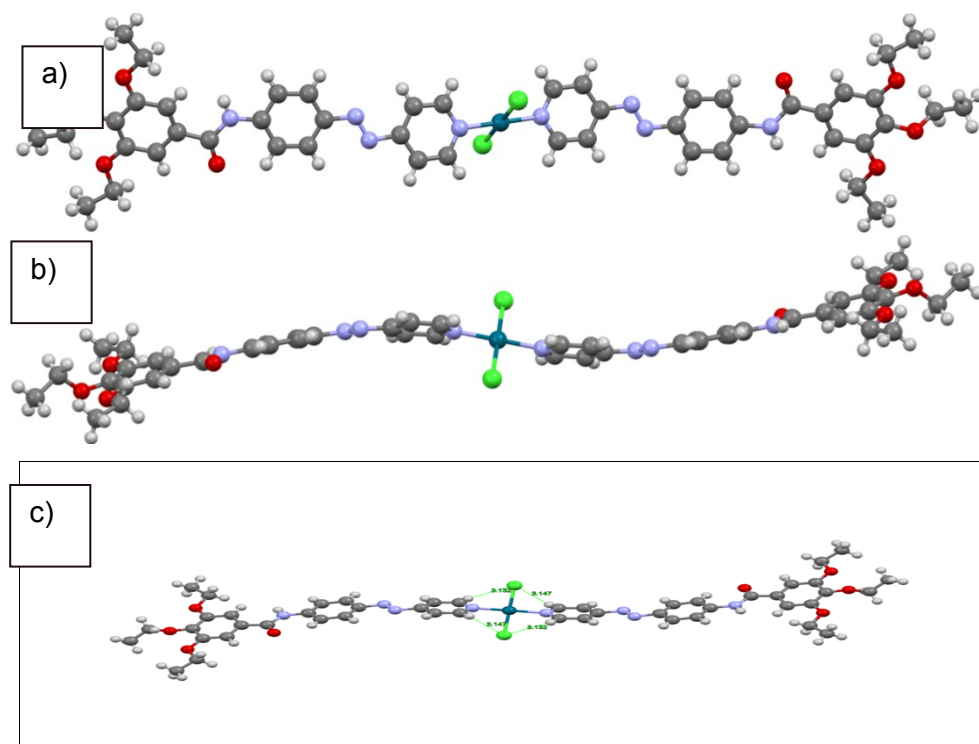


Fig. S18. Crystal structure of C_2 in three different views (front, side and diagonal views).

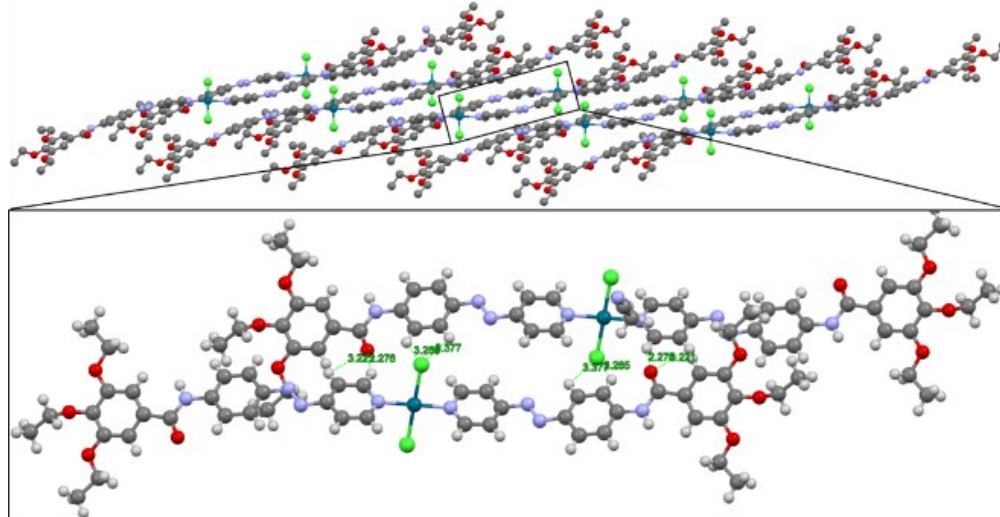


Fig. S19. Packing of C_2 in b -axis and c -axis directions together with 4 $C-H \cdots Cl$ and one $C-H \cdots O$ intermolecular interactions between adjacent molecules.

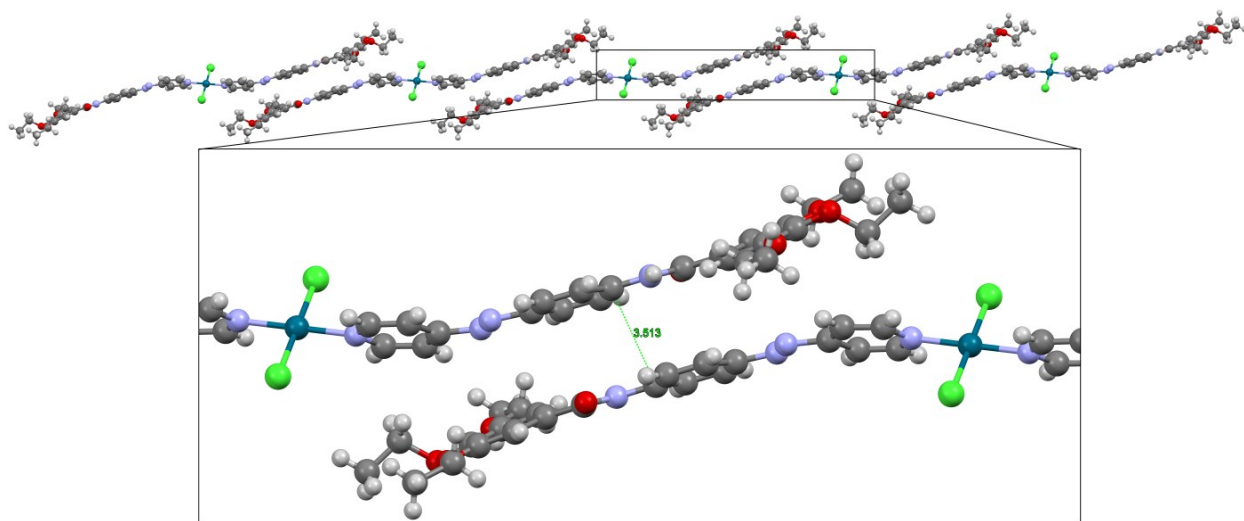


Fig. S20. Packing of molecules of C_2 along a -axis via π - π interactions.

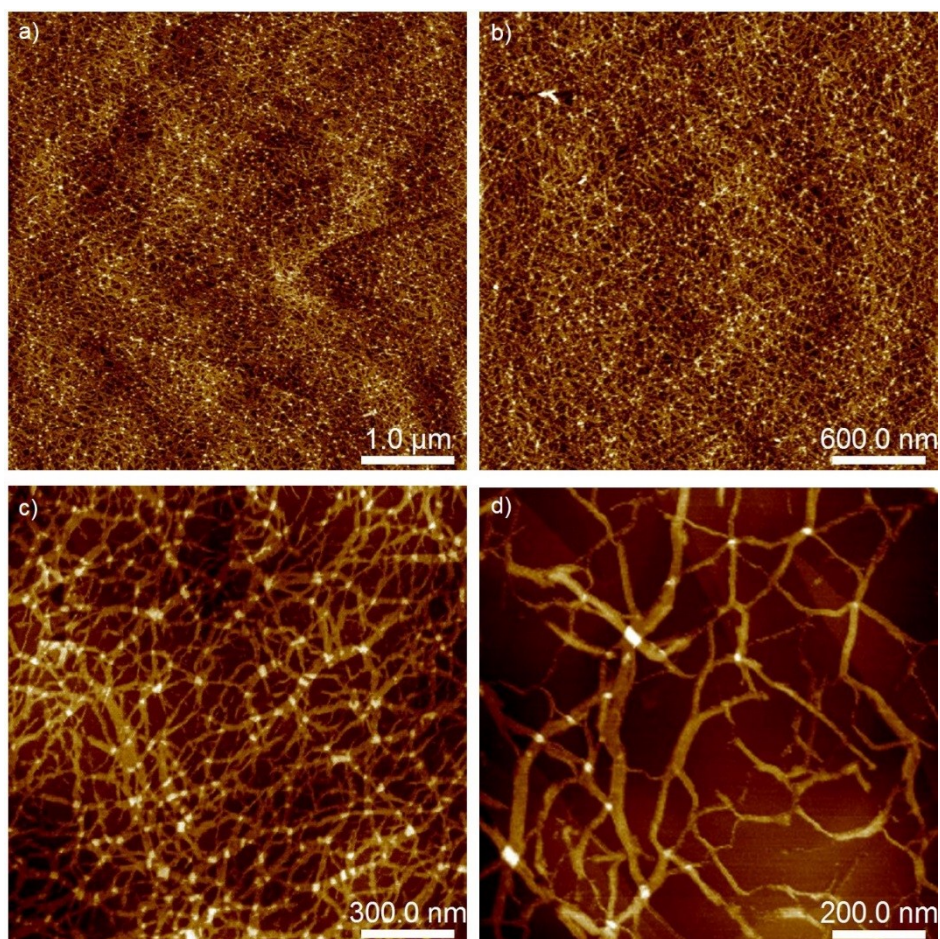


Figure S21. AFM images of C_1 (5×10^{-5} M) aggregates in MCH at 283 K on HOPG.

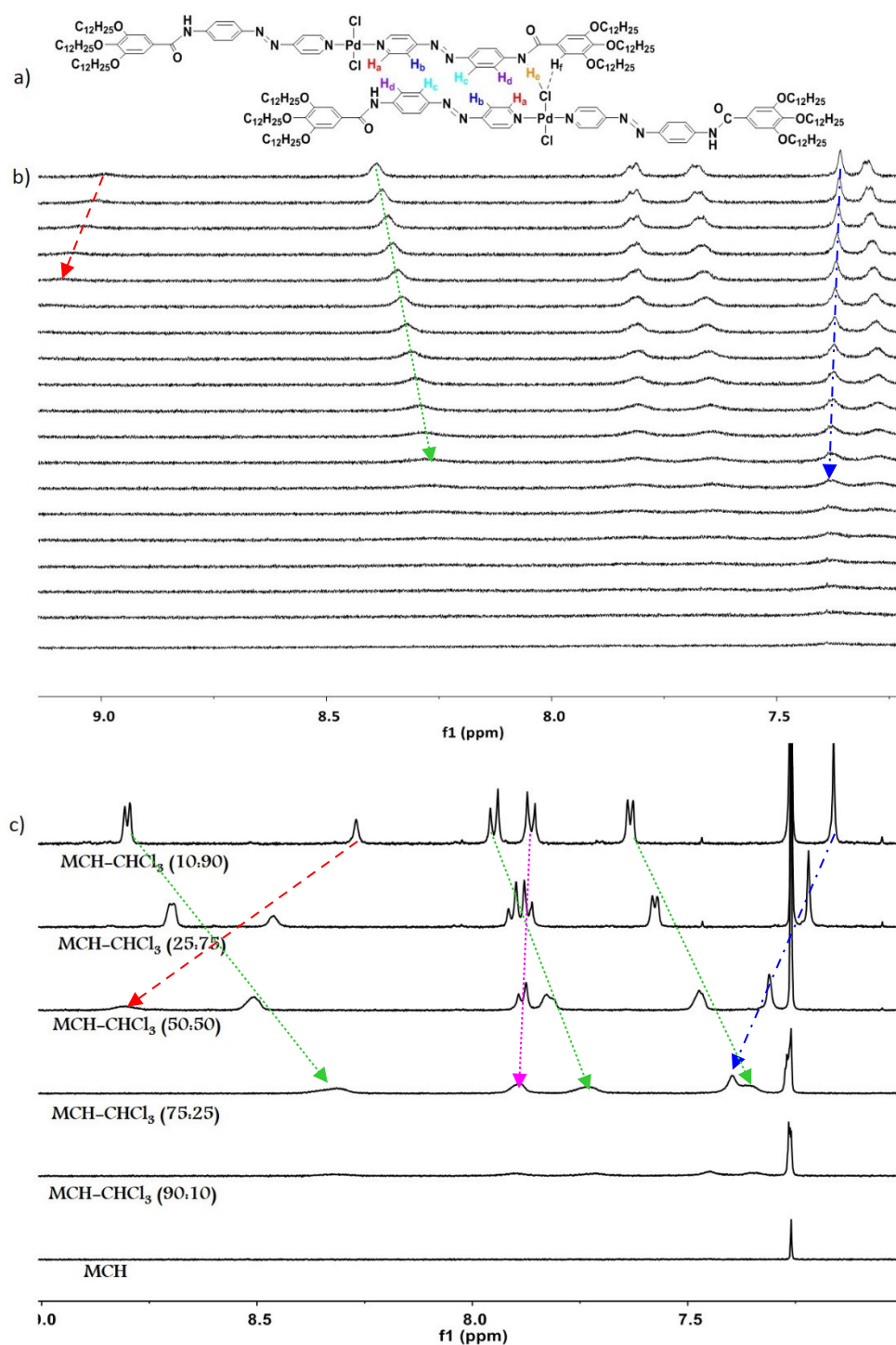


Fig. S22. a) Proposed packing showing the possible π - π , $C-H \cdots Cl$ and $N-H \cdots Cl$ interactions upon aggregation of C_1 . b) Variable temperature (from 328 K to 283 K-top to bottom) 1H NMR of C_1 at 0.5 mM in $MCH-d_{14}:CDCl_3$ (9:1). c) 1H NMR of C_1 in different ratios of $MCH-d_{14}:CDCl_3$ at 299 K. Arrows show the chemical shift corresponding to C_1 -aggregation. Red ($N-H_e \cdots Cl$), Blue ($C-H_f \cdots Cl$) pink ($C-H_d \cdots Cl$) and green (π - π stacking for all other protons).

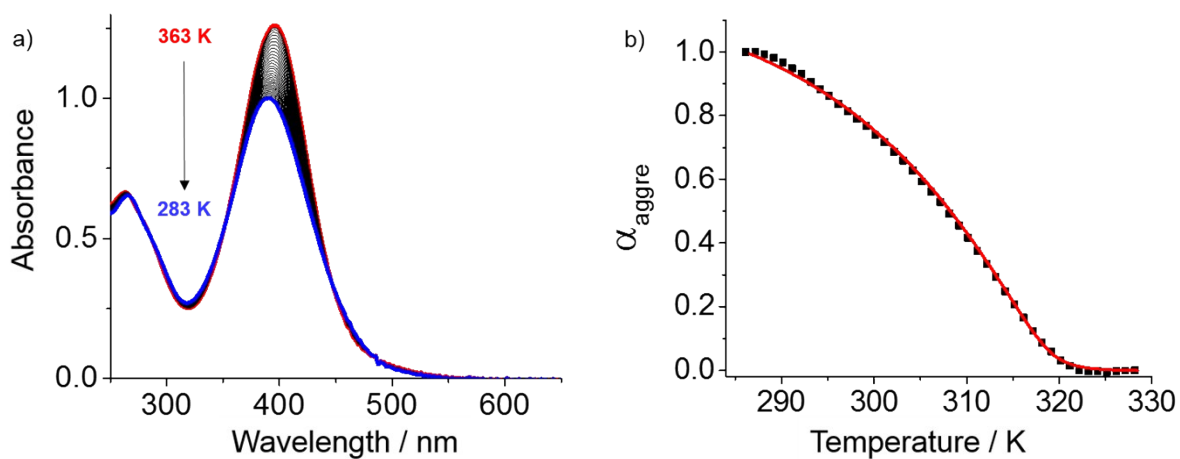


Fig. S23. a) Variable temperature (363 K-283 K) UV-Vis spectra of C_1 at 5×10^{-5} M in MCH-CHCl₃ (9:1) and b) Cooling curve of C_1 obtained by monitoring the absorbance at 395 nm (black dots) and fit to the cooperative model (red line).

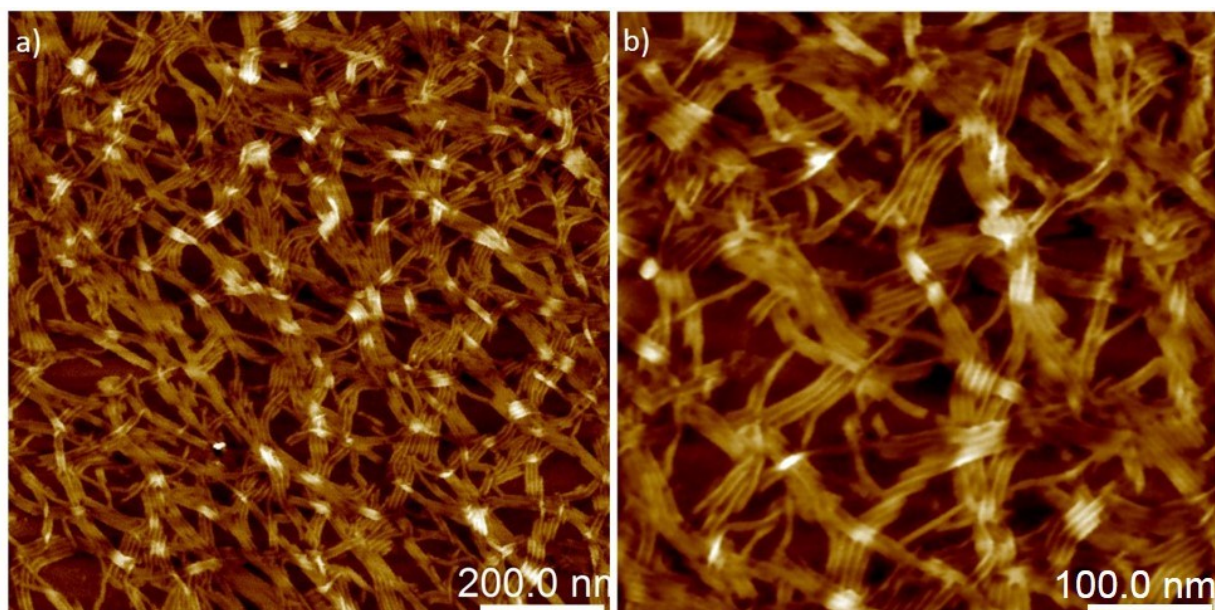


Fig. S24. AFM images of C_1 (5×10^{-5} M) aggregates formed in MCH-CHCl₃ (9:1) at 283 K on HOPG.

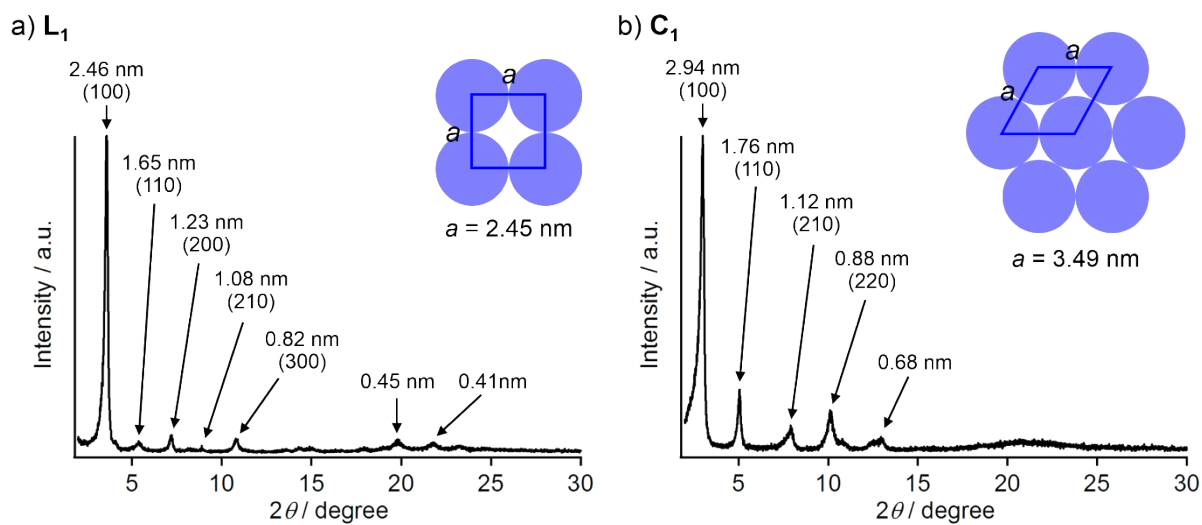


Fig. S25. PXRD patterns of films of a) L_1 and b) C_1 . The films were prepared by drop-casting a) MCH solution of L_1 (5×10^{-3} M) and b) MCH/ $CHCl_3$ (90:10) of C_1 (5×10^{-3} M), respectively.

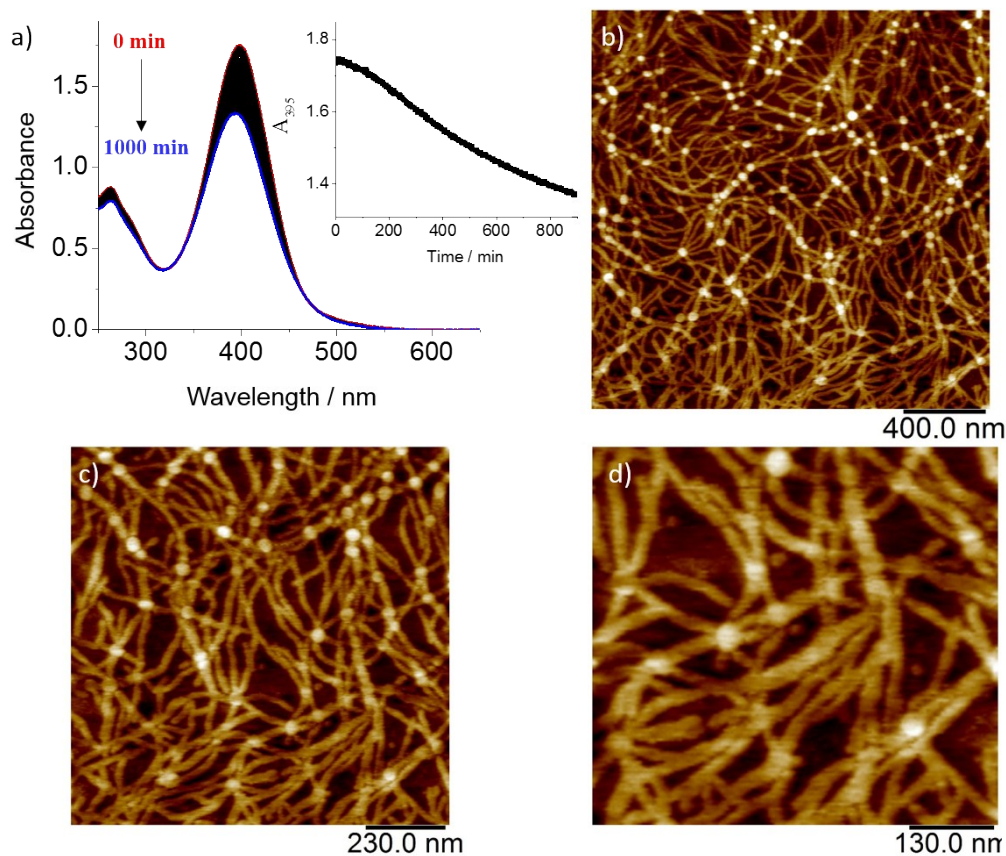


Fig. S26. a) Time-dependent UV-Vis absorption changes of fast cooled C_1 (5×10^{-5} M) a) from 0 to 1000 min in MCH- $CHCl_3$ (9:1) at 283 K; inset: plot of A_{395} vs. time ($l = 1$ mm). b-d) corresponding AFM images on HOPG after keeping at 283 K for 1000 min.

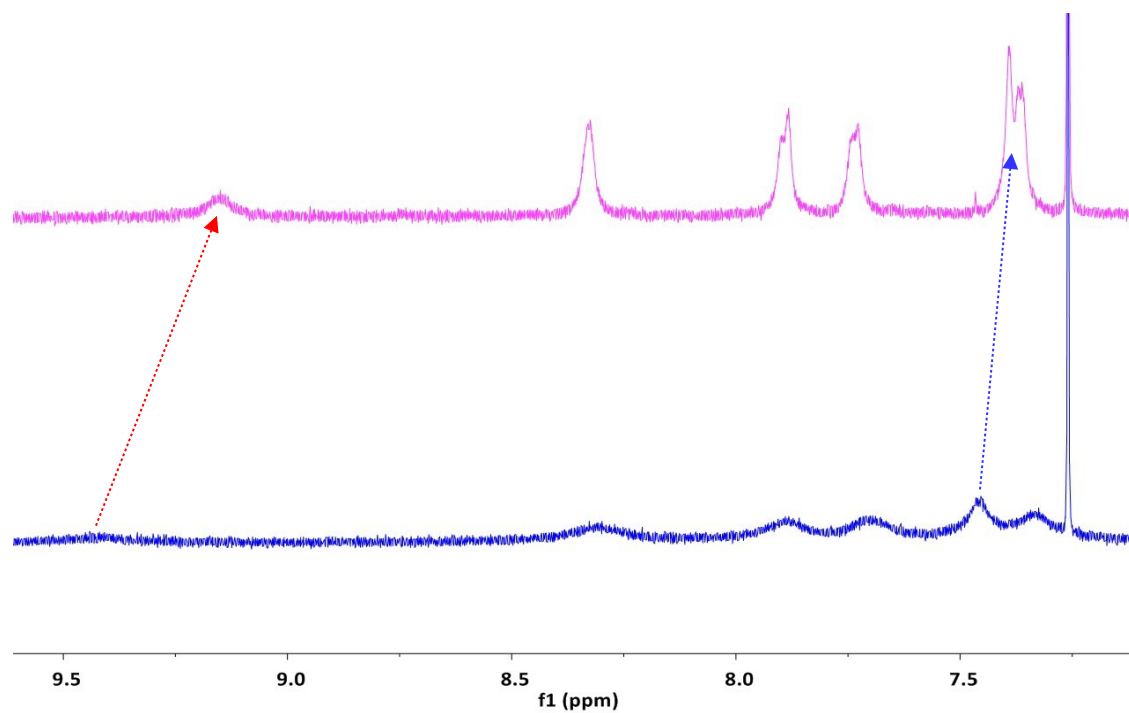


Fig. S27. ¹H-NMR changes of **C**₁ (5×10^{-4} M) in MCH-*d*₁₄-CDCl₃ (9:1) before (blue) and after (pink) irradiation for 30 min with a 365 nm LED lamp at 299 K. Arrows show the chemical shift corresponding to N-H···Cl and CH···Cl dissociation.

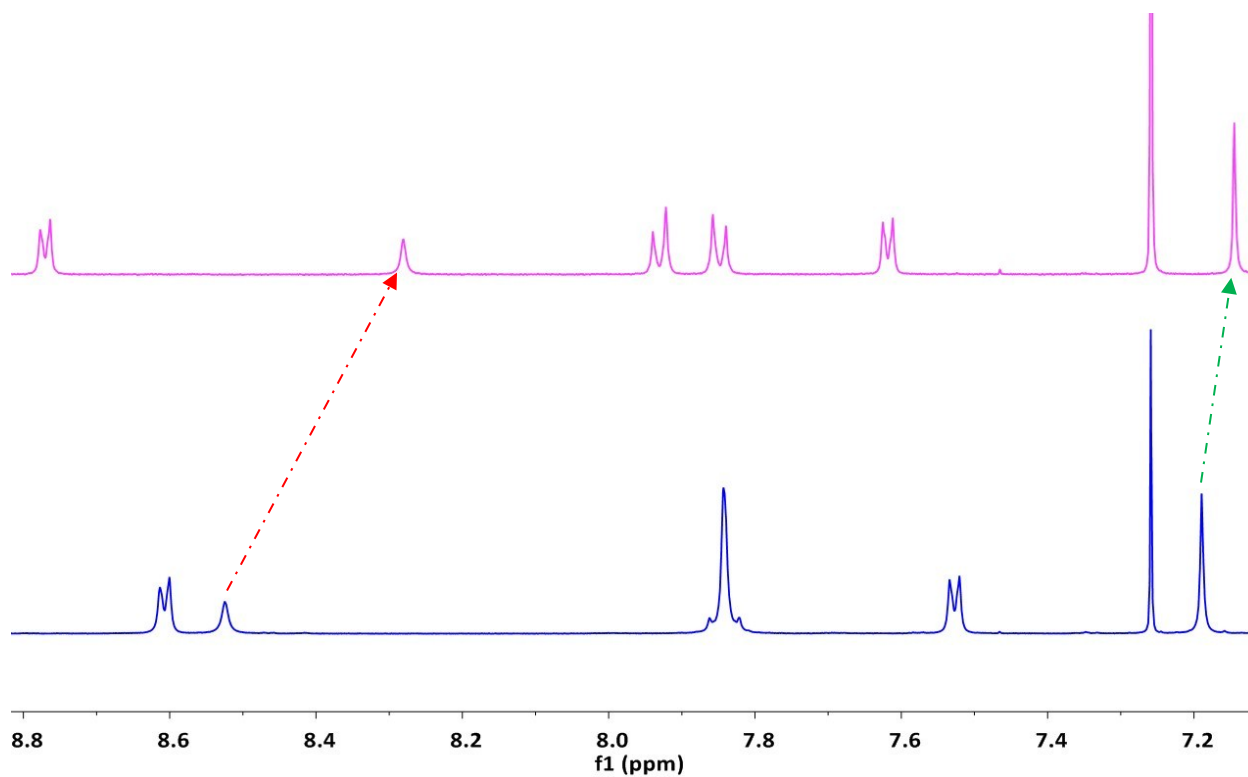


Fig. S28. ¹H-NMR changes of **C**₁ (9 mM) in CDCl₃ before (blue) and after (pink) irradiation for 30 min with a 365 nm LED lamp at 299 K. Arrows show the chemical shifts corresponding to N-H···Cl (red) and C-H···Cl (green) dissociation.

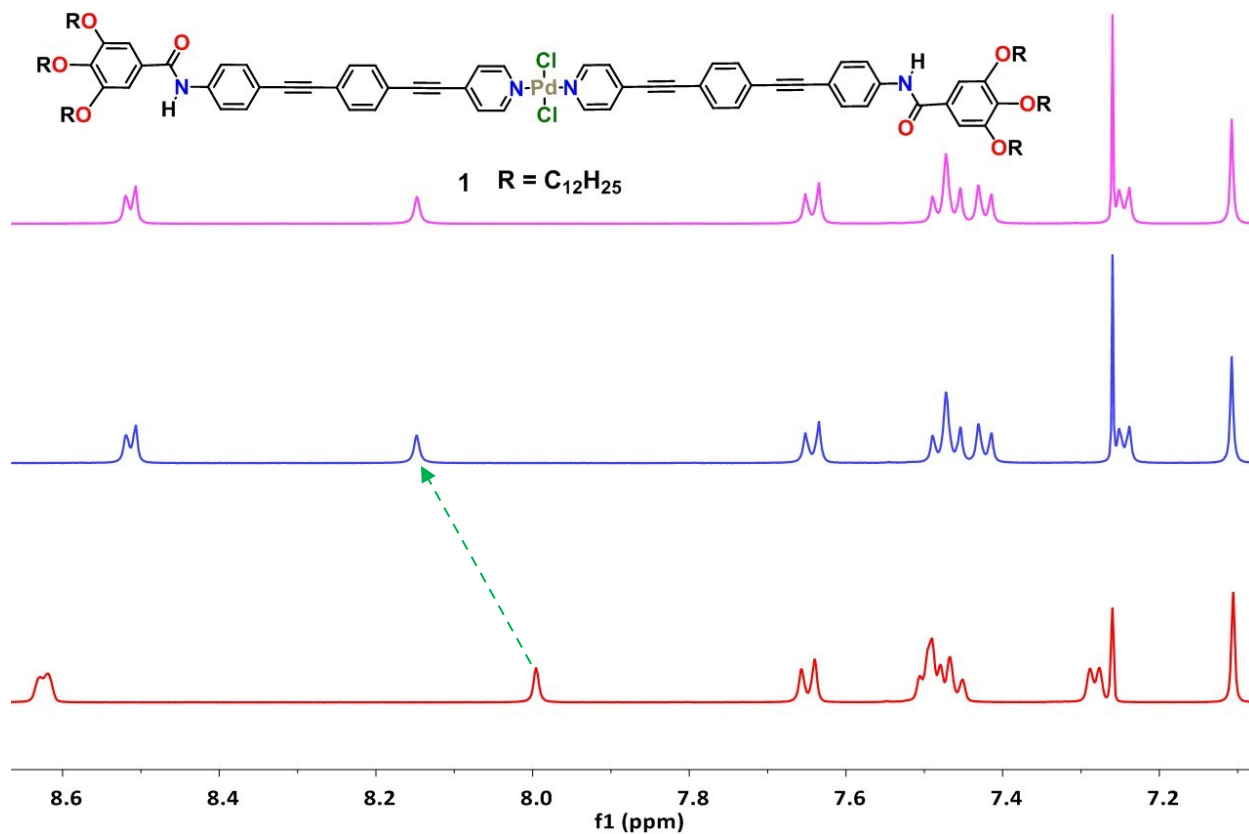


Fig. S29. ¹H-NMR changes of **1** (9 mM) in CDCl₃ showing self-assembly upon cooling from 323 K (red) to 299 K (blue) which remain unaltered after (pink) irradiation for 30 min with a 365 nm LED lamp. Green arrow show the chemical shift corresponding to N-H...Cl formation.

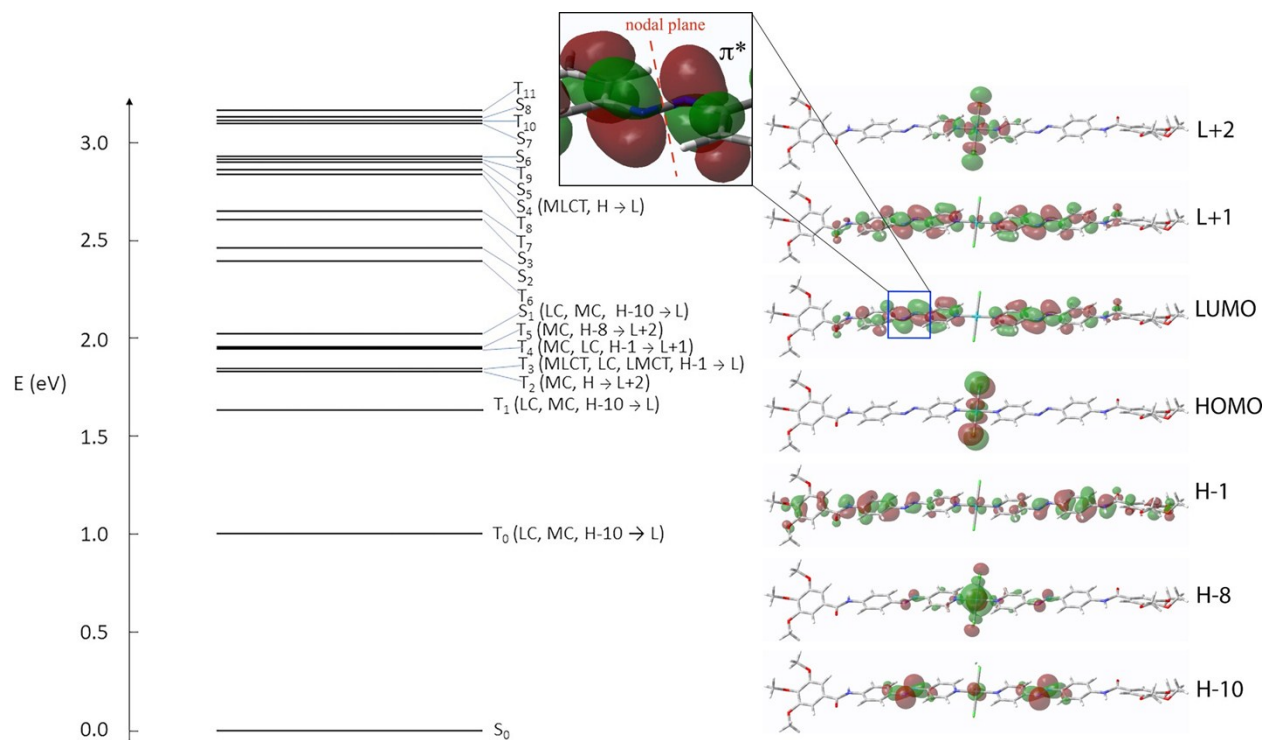


Fig. S30. Triplet (T) and Singlet (S) excited states and corresponding molecular orbitals predicted for the *Trans* isomer with anti-parallel amides. The numbers beside the levels represent the molecular orbitals with the largest contribution to the state, where $H = \text{HOMO}$ and $L = \text{LUMO}$. MC = metal centered, LC = ligand centered, MLCT = metal-to-ligand charge transfer, XLCT = halogen-ligand charge transfer, XC = halogen centered. All calculations were done at the DFT/TDDFT level (PBE0/6-31G*/LANL2DZ) in vacuum. Inset: LUMO electron density of the *Trans* isomer with antiparallel amides predicted from DFT (PBE0/6-31G*/LANL2DZ) calculations in vacuum. This π molecular orbital is anti-bonding with respect to the N=N double bond, and population of this orbital via light irradiation breaks that double bond, allowing then the free rotation around the N-N single bond.

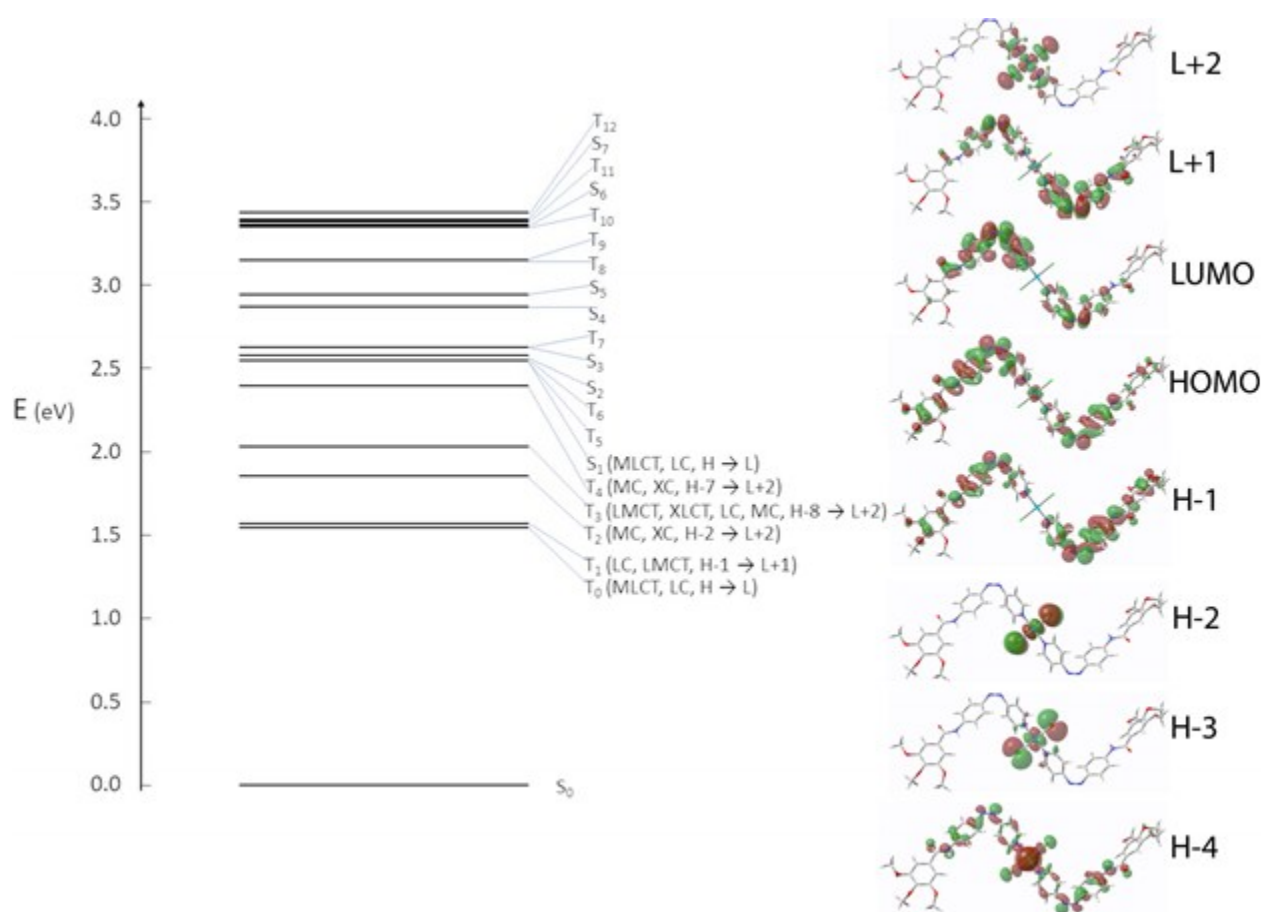


Fig. S31. Triplet (T) and Singlet (S) excited states and corresponding molecular orbitals predicted for the Cis isomer. The numbers beside the levels represent the molecular orbitals with the largest contribution to the state, where H = HOMO and L = LUMO. MC = metal centered, LC = ligand centered, MLCT = metal-to-ligand charge transfer, XLCT = halogen-ligand charge transfer, XC = halogen centered. All calculations were done at the DFT/TDDFT level (PBE0/6-31G*/LANL2DZ) in vacuum.

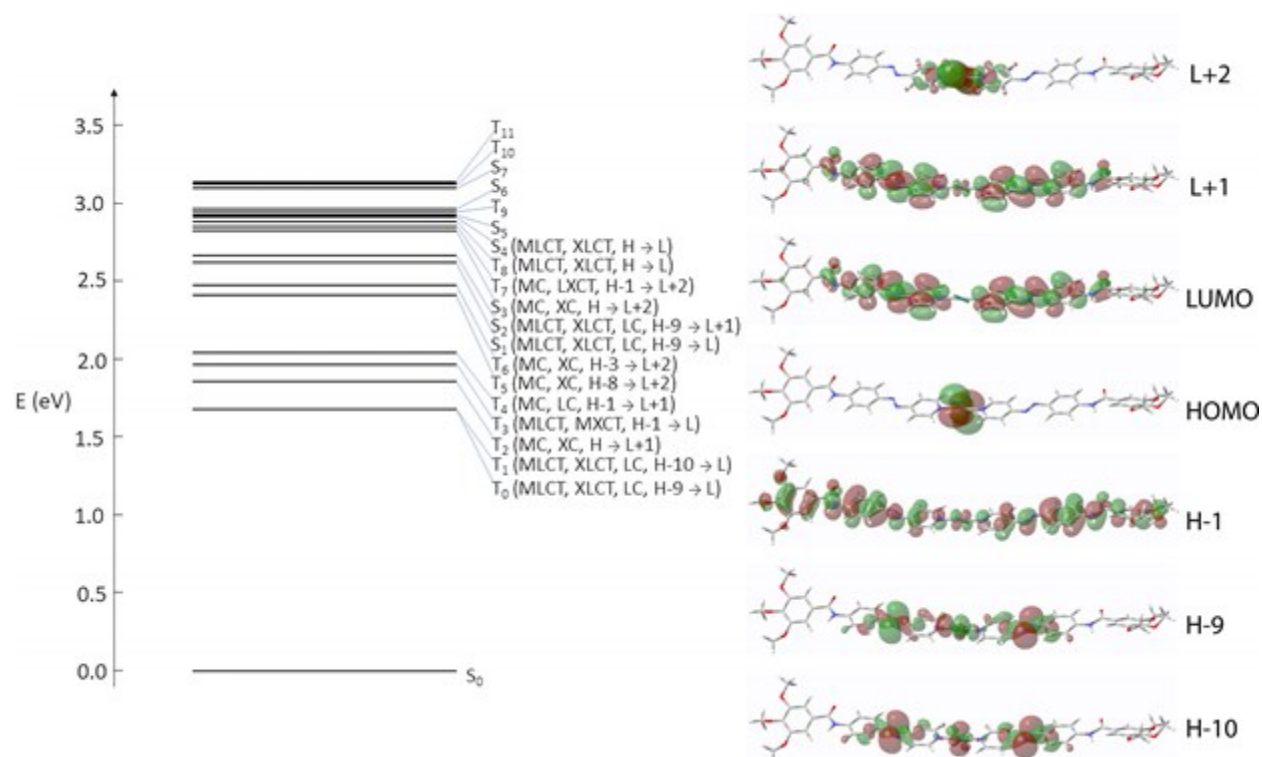


Fig. S32. Triplet (T) and Singlet (S) excited states and corresponding molecular orbitals predicted for the Trans isomer with parallel amides. The numbers beside the levels represent the molecular orbitals with the largest contribution to the state, where H = HOMO and L = LUMO. MC = metal centered, LC = ligand centered, MLCT = metal-to-ligand charge transfer, XLCT = halogen-ligand charge transfer, XC = halogen centered. All calculations were done at the DFT/TDDFT level (PBE0/6-31G*/LANL2DZ) in vacuum.

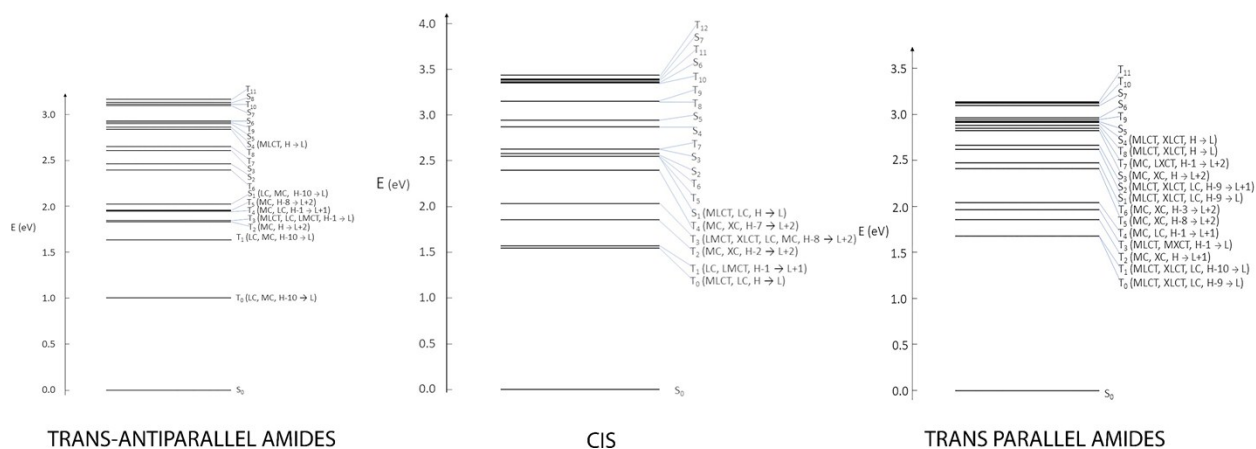


Fig. S33. Triplet (T) and Singlet (S) excited states predicted for the Cis and both Trans (parallel and antiparallel amides) isomers. The numbers beside the levels represent the molecular orbitals with the largest contribution to the state, where H = HOMO and L = LUMO. MC = metal centered, LC = ligand centered, MLCT = metal-to-ligand charge transfer, XLCT = halogen-ligand charge transfer, XC = halogen centered. All calculations were done at the DFT/TDDFT level (PBE0/6-31G*/LANL2DZ) in vacuum.

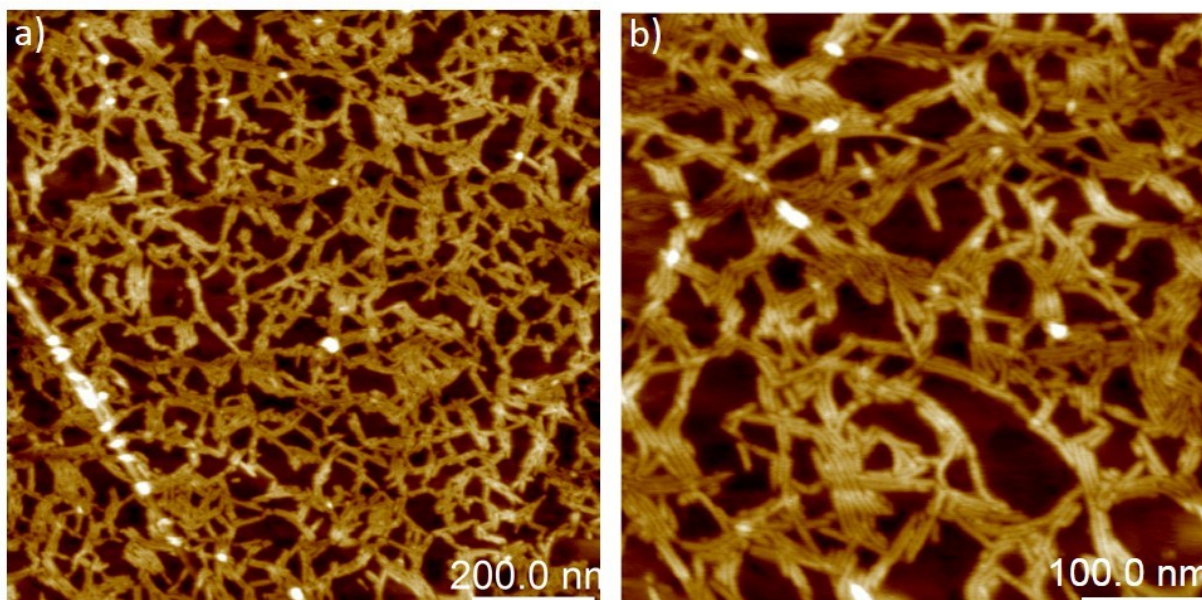


Fig. S34. AFM images of C_1 (5×10^{-5} M) aggregates formed in MCH- $CHCl_3$ (9:1) on HOPG upon keeping at 283 K for 800 min after UV-irradiation for 30 min.

References:

- [S1] J. Řezáč, P. Hobza, *J. Chem. Theory Comput.* **2012**, *8*, 141-151.
- [S2] Gaussian 16, Revision B.01, Frisch, M. J.; Trucks, G. W.; Schlegel, H. B.; Scuseria, G. E.; Robb, M. A.; Cheeseman, J. R.; Scalmani, G.; Barone, V.; Petersson, G. A.; Nakatsuji, H.; Li, X.; Caricato, M.; Marenich, A. V.; Bloino, J.; Janesko, B. G.; Gomperts, R.; Mennucci, B.; Hratchian, H. P.; Ortiz, J. V.; Izmaylov, A. F.; Sonnenberg, J. L.; Williams-Young, D.; Ding, F.; Lipparini, F.; Egidi, F.; Goings, J.; Peng, B.; Petrone, A.; Henderson, T.; Ranasinghe, D.; Zakrzewski, V. G.; Gao, J.; Rega, N.; Zheng, G.; Liang, W.; Hada, M.; Ehara, M.; Toyota, K.; Fukuda, R.; Hasegawa, J.; Ishida, M.; Nakajima, T.; Honda, Y.; Kitao, O.; Nakai, H.; Vreven, T.; Throssell, K.; Montgomery, J. A., Jr.; Peralta, J. E.; Ogliaro, F.; Bearpark, M. J.; Heyd, J. J.; Brothers, E. N.; Kudin, K. N.; Staroverov, V. N.; Keith, T. A.; Kobayashi, R.; Normand, J.; Raghavachari, K.; Rendell, A. P.; Burant, J. C.; Iyengar, S. S.; Tomasi, J.; Cossi, M.; Millam, J. M.; Klene, M.; Adamo, C.; Cammi, R.; Ochterski, J. W.; Martin, R. L.; Morokuma, K.; Farkas, O.; Foresman, J. B.; Fox, D. J. Gaussian, Inc., Wallingford CT, **2016**.
- [S3] (a) Adamo, C.; Barone, V. *J. Chem. Phys.* **1999**, *110*, 6158-6170. (b) Perdew, J. P.; Burke, K.; Ernzerhof, M. *Phys. Rev. Lett.* **1996**, *77*, 3865-3868.
- [S4] (a) Hay, P. J.; Wadt, W. R. *J. Chem. Phys.* **1985**, *82*, 299-310. (b) Hay, P. J.; Wadt, W. R. *J. Chem. Phys.* **1985**, *82*, 270-283. (c) Wadt, W. R.; Hay, P. J. *J. Chem. Phys.* **1985**, *82*, 284-298.
- [S5] MOPAC2016, James J. P. Stewart, Stewart Computational Chemistry, Version 7.263W, web: [HTTP://OpenMOPAC.net](http://OpenMOPAC.net)
- [S6] Abraham, M. J.; Murtola, T.; Schulz, R.; Páll, S.; Smith, J. C.; Hess, B.; Lindahl, E. *SoftwareX* **2015**, *1-2*, 19-25.
- [S7] Humphrey, W.; Dalke, A.; Schulten, K. *J. Mol. Graph.* **1996**, *14*, 33-38.
- [S8] http://homepage2.nifty.com/~hsc/soft/cellcalc_e.html